Universidade de Aveiro
Ano 2024

Sílvia Filipa Ventura da Silva

Deteção móvel multiparamétrica através da termometria por luminescência para e-saúde

Multiparametric mobile sensing through luminescence thermometry for e-health

Universidade de Aveiro
Ano 2024

Sílvia Filipa Ventura da Silva

Deteção móvel multiparamétrica através da termometria por luminescência para e-saúde

Multiparametric mobile sensing through luminescence thermometry for e-health

Dissertação apresentada à Universidade de Aveiro para cumprimento dos requisitos necessários à obtenção do grau de Mestre em Engenharia Biomédica, realizada sob a orientação científica da Doutora Maria Rute de Amorim e Sá Ferreira André, Professora Catedrática do Departamento de Física da Universidade de Aveiro e do Doutor Albano Neto Carneiro Neto, Investigador do Departamento de Física e CICECO-Instituto de Materiais de Aveiro da Universidade de Aveiro.

This work was developed within the scope of the project CICECO-Aveiro Institute of Materials, UIDB/50011/2020, UIDP/50011/2020 & LA/P/0006/2020, financed by national funds through the FCT/MCTES (PIDDAC) financed by national funds through the FCT/MEC (PIDDAC), and when appropriate co-financed by FEDER under the PT2020 Partnership through European Regional Development Fund (ERDF) in the frame of Operational Competitiveness and Internationalization Programme (POCI).

Dedico este trabalho ao meu futuro eu e à minha família.

o júri

presidente

Professor Doutor Carlos Davide da Rocha Azevedo
Professor Auxiliar da Universidade de Aveiro

vogais

Professora Doutora Maria Rute de Amorim e Sá Ferreira André
Professora Catedrática da Universidade de Aveiro

Doutora Nélia Jordão Alberto
Investigadora Auxiliar do Instituto de Telecomunicações, Universidade de Aveiro

agradecimentos

Agradeço aos meus orientadores, Doutora Maria Rute de Amorim e Sá Ferreira André e Doutor Albano Neto Carneiro Neto. A orientação, a dedicação e a disponibilidade constante destes foram essenciais para o sucesso desta dissertação.

Também agradeço aos Mestres Gonçalo Figueiredo e Lília Dias, e à Doutora Sandra Correia, pelo auxílio e atenção ao longo deste processo.

Por fim, mas não menos importante, agradeço à minha família, ao meu namorado e aos meus amigos pelo apoio incondicional. A presença destes foi fundamental para a minha motivação e foco ao longo desta jornada.

palavras-chave Temperatura; termometria de luminescência; deteção móvel; etiquetagem inteligente; e-saúde, m-saúde

resumo O desenvolvimento de sensores para a monitorização da temperatura é essencial no campo da engenharia biomédica, em particular no domínio da saúde digital (e-saúde), onde a integração de tecnologia móvel pode contribuir para a melhoria da prestação de cuidados de saúde. A temperatura é um parâmetro fisiológico fundamental que fornece informações valiosas sobre a saúde de um indivíduo e ajuda no diagnóstico, tratamento e prevenção de uma vasta gama de condições médicas. Entre as várias técnicas de medição da temperatura, a termometria de luminescência destaca-se pela sua natureza remota e facilidade de uso. A termometria de luminescência tem o potencial de revolucionar as metodologias de deteção de temperatura, aproveitando as propriedades únicas dos materiais luminescentes, como a sua sensibilidade às mudanças de temperatura e a compatibilidade com dispositivos portáteis como os telemóveis. Esta inovação permite o avanço de novos sensores na área da monitorização móvel promovendo o progresso em muitos campos, e contribuindo, assim, para a melhoria da qualidade de vida. Esta dissertação investiga as capacidades de termometria luminescente móvel, usando materiais biocompatíveis, tais como pontos de carbono (CDs) que apresentam propriedades de luminescência dependentes da temperatura. Todas as amostras exibem um comportamento de emissão de fosforescência, na ordem de segundos, permitindo que o tempo de aquisição da emissão seja incluído como um parâmetro adicional juntamente com o parâmetro termométrico (Δ) raciométrico associado à intensidade da emissão. Esta abordagem multiparamétrica permite aumentar a sensibilidade do termómetro, criando parâmetros raciométricos distintos em função da temperatura (T em ºC) e do tempo de atraso na leitura (t em s), $\Delta(T, t)$. O mecanismo de emissão foi detalhado, tendo por base a fosforescência retardada ativada termicamente (TADP). Diferentes misturas físicas de CDs funcionalizados com diferentes moléculas orgânicas, permitem modular o efeito TADP. Foram analisados cerca de 100 parâmetros termométricos na região entre 23 e 45 ºC, revelando valores de sensibilidade relativa elevada ($7{,}9\% \cdot {}^{\circ}C^{-1}$). A combinação da deteção usando um espectómetro portátil e um telemóvel, tornam a termometria luminescente mais versátil e acessível. A integração da termometria de luminescência com a tecnologia móvel abre novas possibilidades para a monitorização contínua da saúde e para a telemedicina, promovendo a e-saúde.

keywords temperature; luminescence thermometry; mobile sensing; smart labeling; e-health, m-health

abstract The development of temperature sensors is pivotal in biomedical engineering, particularly within the realm of digital health (e-health), where integrating technology enhances healthcare delivery. Temperature is a critical physiological parameter that provides valuable insights into an individual's health, aiding in the diagnosis, treatment, and prevention of various medical conditions. Among temperature measurement techniques, luminescence thermometry stands out for its non-invasive nature and ease of use. Luminescence thermometry, leveraging the unique properties of luminescent materials, offers an intriguing approach to thermal sensing due to its sensitivity to temperature changes and compatibility with portable devices like smartphones. This innovation facilitates the development of advanced sensors for mobile monitoring, driving progress across multiple fields and improving quality of life. This dissertation investigates the potential of mobile luminescence thermometry using biocompatible materials such as carbon dots, which exhibit luminescence properties dependent on temperature. All samples demonstrated long-lived phosphorescence behavior (in the order of seconds), allowing the integration of emission acquisition time into the ratiometric temperature parameter (Δ). This multiparametric approach will optimize the thermal response and enhance sensitivity, creating distinct ratiometric parameters that can be found as a function of the temperature (T in ºC) and delay time (t in s), $\Delta(T, t)$. The emission mechanism is elucidated through thermally activated delayed phosphorescence (TADP). By modulating the TADP effect through different CD mixtures, we analyzed approximately 100 thermometric parameters within the 23 to 45 ºC range, revealing relatively high sensitivity values ($7{,}9\% \cdot {}^{\circ}C^{-1}$). Utilizing a portable spectrophotometer and a mobile device for detection enhances the accessibility and versatility of luminescent thermometry. The integration of luminescence thermometry with mobile technology opens up new possibilities for continuous health monitoring and telemedicine.

reconhecimento do uso de ferramentas IA

Reconhecimento do uso de tecnologias e ferramentas de Inteligência Artificial (IA) generativa, softwares e outras ferramentas de apoio.

Reconheço o uso de *QuillBot* (https://quillbot.com) para melhorar a linguagem escrita, nomeadamente, correção de gralhas e erros gramaticais em algumas frases ao longo desta dissertação. Reconheço a utilização do *Matlab*® como ferramenta para efetuar a análise RGB. Reconheço o uso de *Python* para criar um código para efetuar uma análise exaustiva dos dados, envolvendo tarefas como a interpolação 2D de pontos, cálculos de derivadas numéricas e geração de resultados.

Index

List of Acronyms

AIS	Aggregation-induced state
B	Blue coordinate intensity
BA	Boric acid
CD_A	Carbon dots produced from Dibenzoylmethane
CD_B	Carbon dots produced from Rhodamine B
CD_{AB}	CD_A and CD_B mixtures
CDs	Carbon Dots
CD_{11}	CD_A and CD_B mixture in a weight ratio (A:B) of 1:1
CD_{14}	CD_A and CD_B mixture in a weight ratio (A:B) of 1:4
CD_{41}	CD_A and CD_B mixture in a weight ratio (A:B) of 4:1
DBM	Dibenzoylmethane
EtOH	Ethanol
G	Green coordinate intensity
IC	Internal conversion
IoT	Internet of Things
ISC	Intersystem crossing
I(T)	Emitted intensity change
I_A	CD_A integrated intensity area
I_B	CD_B integrated intensity area
I_A^1	CD_A integrated intensity area between 389-470 nm
I_A^2	CD_A integrated intensity area between 470-841 nm
I_B^1	CD_B integrated intensity area between 389-500 nm
I_B^2	CD_B integrated intensity area between 500-841 nm
I_{AB}	CD_{AB} integrated intensity area
I_{AB}^1	CD_{AB} integrated intensity area between 389–450 nm
I_{AB}^2	CD_{AB} integrated intensity area between 450-575 nm
I_{AB}^3	CD_{AB} integrated intensity area between 575-841 nm
I_{11}^1	CD_{11} integrated intensity area between 389–450 nm
I_{11}^2	CD_{11} integrated intensity area between 450-575 nm
I_{11}^3	CD_{11} integrated intensity area between 575-841 nm
I_{14}^1	CD_{14} integrated intensity area between 389–450 nm

I_{14}^{2}	CD_{14} integrated intensity area between 450-575 nm
I_{14}^{3}	CD_{14} integrated intensity area between 575-841 nm
I_{41}^{1}	CD_{41} integrated intensity area between 389–450 nm
I_{41}^{2}	CD_{41} integrated intensity area between 450-575 nm
I_{41}^{3}	CD_{41} integrated intensity area between 575-841 nm
LEDs	Light emitting diodes
Ln^{3+}	Lanthanide
MOFs	Metal-organic frameworks
NaOH	Sodium hydroxide
NIR	Near-infrared region
NTC	Thermistor with a negative temperature coefficient
PTC	Thermistor with a positive temperature coefficient
QDs	Semiconductor quantum dots
QY	Quantum yield
R	Repeatability
R_{mean}	Red coordinate intensity mean
RGB	“Red, Green, Blue”
RhB	Rhodamine B
S_a	Absolute thermal sensitivity
S_r	Relative thermal sensitivity
S_m	Maximum value of S_r
S_1	First singlet state
S_2	Second singlet state
TADP	Thermally activated delayed phosphorescence
TEM	Transmission electron microscopy
T_m	Temperature corresponding to the S_m
T_1	First triplet state
UV	Ultraviolet
$\Delta(T)$	Thermometric parameter
$\tau(T)$	Luminescence lifetime
δT	Temperature resolution
δt	Temporal resolution
δx	Spatial resolution

List of Figures

List of Tables

Chapter 1. Introduction

1.1. Motivation

Advancements in medicine, science, and technology have resulted in extended lifespans and a significant reduction in mortality and morbidity rates attributed to both infectious and non-communicable diseases. As a result, the global population is aging, leading to a higher prevalence of chronic illnesses. This places additional strain on healthcare systems, which now face new obstacles (*1*). The challenges encompass the necessity for innovative technologies, computerized software algorithms, and intelligent devices that can provide continuous monitoring and assistance to patients from anywhere (*2*). Moreover, there is a pressing need for improved access to outpatient care, more efficient and cost-effective healthcare delivery models, initiatives to promote overall health maintenance and restoration, and efforts to increase patient autonomy and independence (*3*). These highlight the critical importance of innovative and sophisticated scientific solutions, which have helped shape the evolution of electronic health (e-health) (*1*),(*3*).

In the era of digital transformation, e-health harnesses the power of digital technologies, such as connected devices, computers, mobile phones, websites, and applications, to enhance healthcare services and information dissemination (*1*). It encompasses multiple applications, ranging from electronic health records, telemedicine, and mobile health (m-health) to health information systems and wearable health monitoring devices (*3*). Despite advancements brought about e-health, challenges persist in the real-time monitoring and management of patient health. Continuous monitoring of daily health data shows promise in disease prediction or early detection, especially for patients with chronic illnesses, mobility limitations, disabilities, post-surgery recovery, newborns, and the elderly (*4*). Furthermore, wireless communication technology and high sensor performance are critical components in health self-monitoring systems. The urgency for improved communication, accelerated by the COVID-19 pandemic, has led to increased adoption of mobile devices and the rise of m-Health (mobile-assisted e-Health) (*5*). Real-time transmission of sensor data to mobile phones enables information dissemination to hospitals and other relevant locations. Globally, mobile and wireless technologies have become ubiquitous, ushering in a new era of healthcare services and improving existing ones. The integration of mobile devices into clinical practice has boosted the availability and quality of medical software applications, including mobile apps, crucial in various aspects of healthcare delivery (6).

Body temperature is an essential aspect of human health surveillance that cannot be overlooked. Controlling and observing body temperature are essential elements in the evolution of e-Health systems (*6*). Real-time and accurate monitoring of body temperature holds significant importance for several reasons. Temperature is a basic vital sign that provides crucial insights into the body's physiological status. Beyond merely indicating fever or illness, subtle changes in body temperature can signify deeper physiological alterations. These fluctuations may indicate the presence of an infection, inflammation, or other underlying health conditions. As a result, precise temperature measurements are critical for diagnosing illnesses, tracking disease progression, and evaluating treatment efficacy. In light of these needs, the development of temperature-sensing technology and control systems that offer high precision, non-invasiveness, affordability, and robust real-time performance has become a key research objective in the field of electronic medicine (*6*). Recent technological developments have revolutionized temperature measurement across various applications, prompting a significant paradigm shift. For instance, the introduction of smart optical

temperature sensors that can be connected to the internet has enabled remote and real-time temperature monitoring (*7*).

As a biomedical engineer, I am dedicated to developing innovative solutions for health challenges and advancing the e-health agenda. My focus is on exploring new avenues in temperature optical sensing to offer alternatives to traditional methods and enhance healthcare outcomes. Luminescence thermometry is particularly promising, leveraging the unique properties of luminescent materials. Their sensitivity to temperature variations and compatibility with portable devices like smartphones make them an intriguing topic for my dissertation.

1.2. Framework and State of the Art

Temperature is one of the most influential and fundamental physical variables, widely utilized across science and technology, accounting for around 80% of the global sensor market (*8*). **Figure 1.1** shows the distribution of different industry sectors for temperature sensors in the global market. Its applications are diverse and include daily life activities, metrology, aerodynamics, climate and marine research, chemistry, medicine, biology, military technology, air conditioning, heating and cooling systems, manufacturing plants, and food and product storage (*9*). It is highly valued and closely monitored in fields such as physics, chemistry, engineering, and environmental science (*10*). Comprehending temperature is a fundamental concept in physics, as it enables the study of the behavior of gases, liquids, and solids. This knowledge is also crucial for disciplines such as thermodynamics and heat transfer, which rely heavily on understanding temperature gradients and thermal energy exchange (*11*). In chemistry, temperature plays an important role in determining the dynamics of chemical reactions. Its effects include changes in reaction rates, equilibrium constants, and ultimately, the overall outcome of the chemical processes (*12*). Precise temperature control is essential in both laboratory and industrial settings to ensure optimal reaction conditions and to maximize the efficiency of chemical processes (*13*). Temperature measurements are used in a variety of engineering applications, such as electronic device thermal management, energy systems, and industrial processes. Temperature monitoring and control are critical to ensuring that equipment and systems operate safely and efficiently (*14*). In environmental science, temperature measurements are crucial for studying climate change, understanding ecosystems, and predicting the behavior of organisms in different environments (*15*).

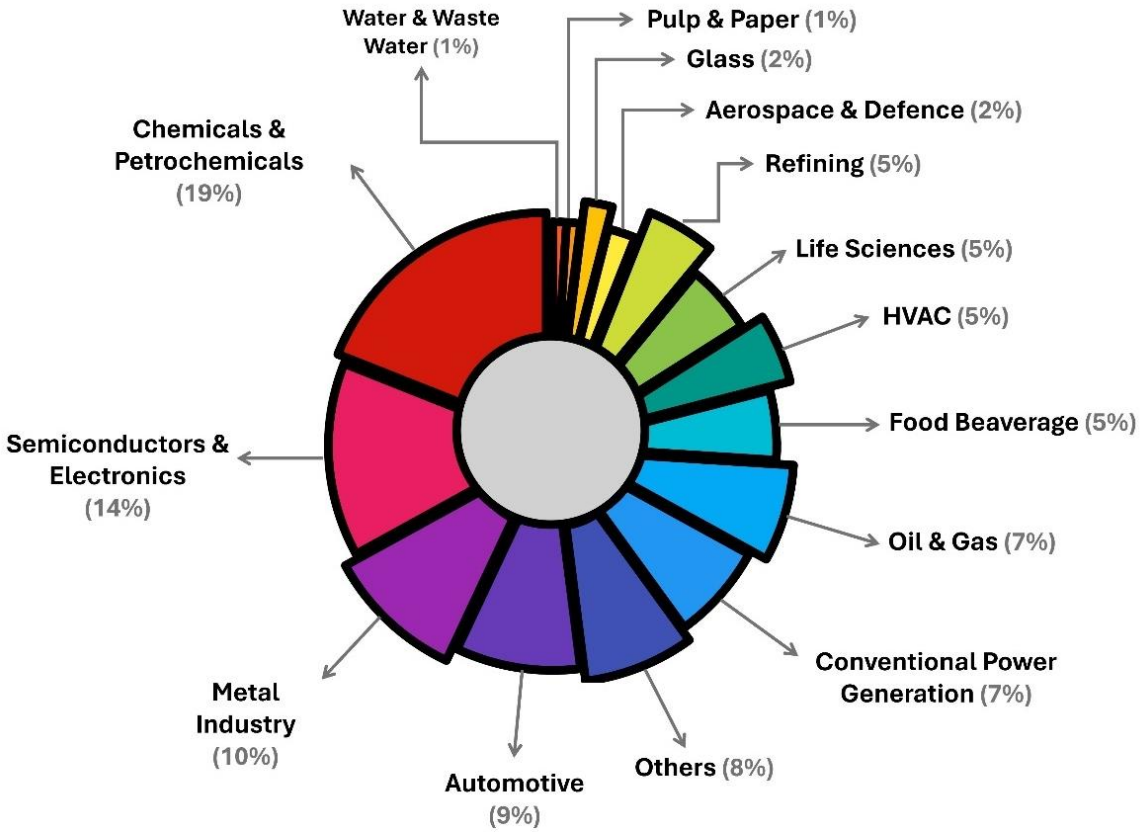

Figure 1.1 Scheme illustrating the generation of revenue for the worldwide market of temperature sensors made in 2015. Adapted from (*8*).

Temperature also plays a vital role in biological processes (*16*), influencing enzyme activity, metabolic rates, and overall organism growth, development, and survival (*17*). Because so many biological processes are temperature-dependent, even minor temperature variations can have a significant impact on biological systems (*17*). With the exception of febrile illness, the temperature of the deep tissues of the body, also known as the body's "core", remains remarkably stable, typically varying by no more than 0.6°C. Despite being exposed to a wide range of external temperatures, the human body maintains a constant core temperature via a sophisticated control system. While the core temperature remains constant, the skin temperature varies in response to environmental conditions, overall health, and the specific region of the body, affecting the body's ability to dissipate heat (*18*). Body temperature is a vital sign that emphasizes the importance of evaluating a person's overall health (*19*). Thus, maintaining optimal body temperature is essential for human comfort (*6*).

The hypothalamus maintains the body temperature of healthy individuals ranging from less than 36.0°C to over 37.5°C when measured orally (*18*). People are considered homeotherms because they maintain relatively constant core body temperatures (*20*). Although the regulatory mechanisms are not perfect, they help maintain a stable body temperature. However, fluctuations may occur during physical activity or exposure to extreme environmental conditions (*18*). During strenuous physical activity, the body generates additional heat, which can temporarily elevate the temperature from 38.3°C to 40°C. Conversely, when exposed to extreme cold, the body's temperature may decrease below 35.6°C (*18*). Heat stress triggers autonomic responses such as cutaneous

vasodilation, which releases heat through radiant and convective heat loss, and sweating, which releases heat through evaporation. Cold stress triggers autonomic responses such as cutaneous vasoconstriction, which helps the body retain heat, as well as metabolic and shivering thermogenesis (*20*). The regulation of body temperature is a homeostatic feedback loop system. The hypothalamus defines the set point, and it is considered here that erroneous signals from central and peripheral temperature receptors are integrated and most effector responses are generated (*20*). Temperature is a key physiological indicator in organisms as various types of cells possess temperature receptors that are associated with multiple biological signaling pathways. Temperature receptors, also called thermoreceptors, are distributed throughout the body and play an important role in maintaining homeostasis, which is the ability of the body to maintain a stable internal environment despite changes in the external environment. These receptors, which act as our temperature sensors, help to regulate various bodily functions, such as blood flow, metabolism, and immune response, by detecting temperature changes (*21*).

However, because the human body's ability to regulate temperature is restricted, monitoring and controlling the environmental temperature is critical for the auxiliary role of medical treatment and the family's daily e-healthcare. Temperatures that are too high or too low are harmful to human health (*6*). Too high a temperature, for example, will place a high load on the thermoregulatory system, reduce the body’s resistance, and cause changes in circulatory, digestive, urinary, and nervous system functions, resulting in increased mortality in cardiovascular, cerebrovascular, diabetes, and other diseases. Too low a temperature can reduce metabolic function, delay pulse and respiration, and promote respiratory tract illness. When the temperature shifts rapidly, the heat-sensitive neurons situated in the front section of the inferior colliculus experience tension, which leads to the body's misalignment and may result in health issues such as asthma, ischemic heart disease, and stroke (*6*).

Monitoring body temperature has been important since ancient times, with physicians in the early Roman Empire recognizing a link between it and poor health. Usually, the body temperature of someone sick is higher than healthy one (*22*). In modern medical applications, thermometry is utilized for the diagnosis and treatment of various diseases, such as stroke, cancer, infections, or inflammations. These conditions can affect the body’s normal temperature-regulating mechanisms, resulting in aberrant temperature variations. Certain kinds of cancer, for example, can increase metabolic activity, leading to an increase in body temperature (*23*). Healthcare providers can more accurately diagnose and treat various conditions by monitoring temperature changes in patients (*24*). Proper temperature monitoring is also crucial as well for detecting deviations from normal temperature values, such as fever, which is a common initial symptom of many illnesses (*22*), including COVID-19, and hyperthermia or hypothermia, which can indicate underlying health issues (*24*). Fever is generally thought to be advantageous in aiding the host in surviving bacterial infections; however, a high fever can also have negative consequences for the host (*25*). Hyperthermia or hypothermia can disrupt enzyme activity in the body, leading to disturbances in human metabolism and resulting in disorders of cells, tissues, and organs. In severe cases, it can even lead to death (*26*). Monitoring temperature can even lead to earlier detection of diseases or conditions in some cases, which can improve patient outcomes and can also be used to monitor patients suffering from chronic illnesses, such as diabetes (*24*). An essential aspect of enhancing e-health involves the monitoring and management of body temperature (*6*). Temperature is one of the most important aspects influencing our health and human well-being, making real-time and reliable monitoring of body temperature, especially important.

The accuracy of temperature measurement techniques can be influenced by numerous factors, including physiological and environmental elements (*17*). These factors encompass the location of measurement, the type of thermometer employed, and environmental conditions such as drafts or humidity levels. Furthermore, physiological factors, such as pathological conditions and health status, including hyperthermia or hypothermia, can also impact measurement accuracy. Anthropological characteristics also complicate the accuracy of body temperature measurements. Variables such as age, sex, body weight, height, and psychological status, along with biorhythmic and menstrual cycle stages, play crucial roles. Additionally, factors such as physical activity level, food intake, measuring modality, time of day, and posture can significantly influence measurement outcomes. To achieve accurate and dependable temperature measurements, it is critical to use the correct measurement techniques and processes (*17*).

The measurement of temperature has its origins in antiquity, with the development of various instruments and methodologies for evaluating body temperature. In the late 16th century, Galileo Galilei created one of the earliest thermometers, and in the early 18th century, Gabriel Fahrenheit invented the mercury-in-glass thermometer. These pioneering devices opened the door to current temperature measurement methods (*22*). An ideal thermometer would possess the physical characteristics of being durable, compact, minimally or non-invasive, reusable, and affordable. The device would offer uninterrupted measurements that would be exact, precise, consistent, and swift. Additionally, would demonstrate a linear or highly predictable reaction and would not need to be calibrated. In practice, these requirements often conflict with each other, as it is unlikely for a device to operate both linearly and with high precision while also providing an accurate and rapid response time (*11*). In this chapter, I will comprehensively investigate a range of thermometers, carefully analyzing their distinct benefits and drawbacks. This thorough analysis will offer a strong and up-to-date overview of this thesis. **Figure 1.2** depicts a timeline of the evolution of thermometers discussed in this dissertation, with a focus on smartphone-based thermometers, denoted as "Mobile".

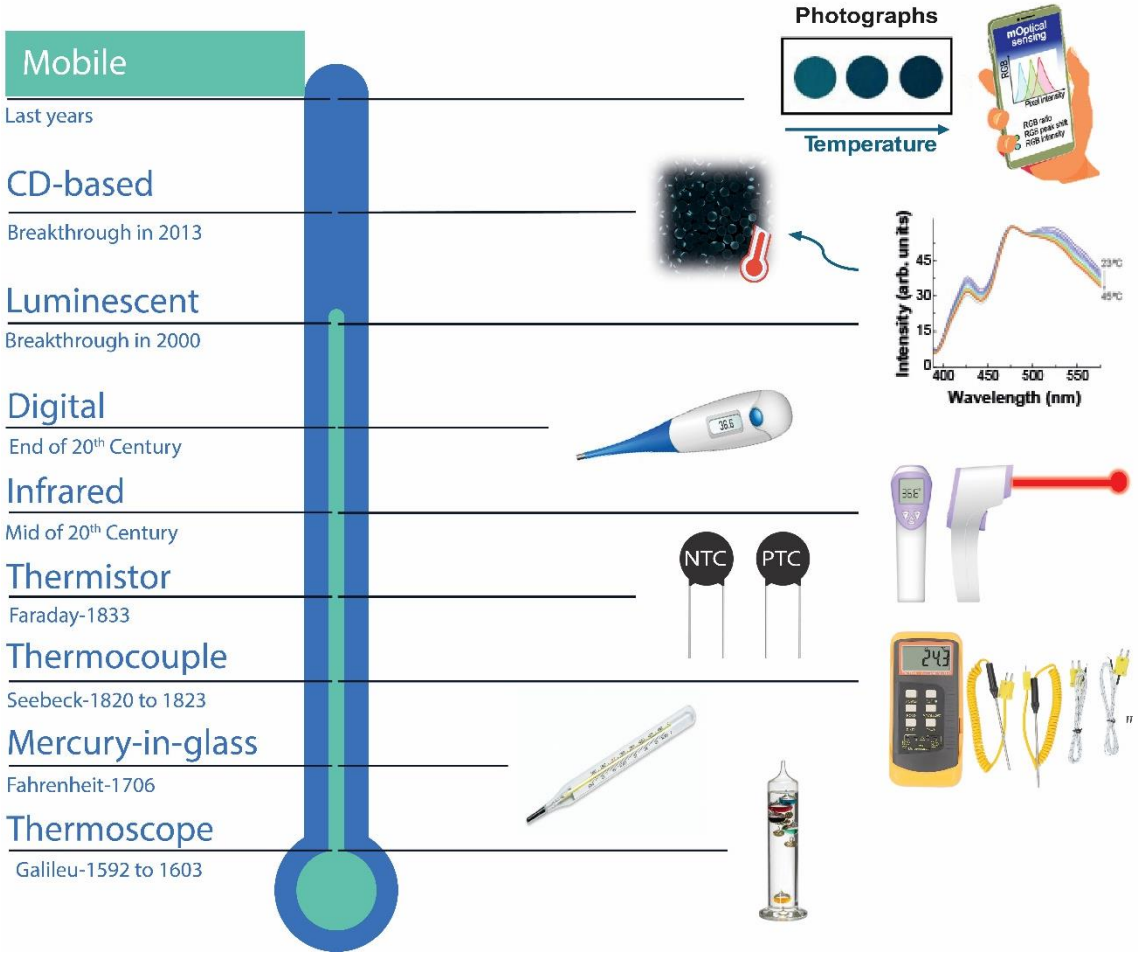

Figure 1.2 Thermometers timeline showing their evolution over the years. The thermometers depicted in the images were sourced from freepik, with the exception of the "Mobile" picture, which was adapted from (*5*).

Conventional temperature sensors are ordinarily referred to as contact thermometers because they assess temperature by directing heat to an intrusive probe (*27*). The three primary heat transmission mechanisms utilized in body temperature measurements are conduction, convection, and radiation. Contact measurement applies the thermal conduction approach by making contact with the temperature transducer to the measurement target position. Non-contact measurements, on the other hand, utilize heat convection and radiation via blood flow and breath gas, as well as photons from electromagnetic waves (*17*). As a result, thermometers can be classified as contact or non-contact based on their physical interaction with the thermistor and the object to be measured (*27*). Thermometers can also be categorized into three types based on the nature of contact between the sensor and the object being measured: non-invasive, semi-invasive, and invasive (*5*). Body temperature is commonly measured using noninvasive methods on the body's surface areas, such as the armpit, groin, outer ear canal, forehead, neck, and chest, using peripheral thermometers (*28*). Semi-invasive methods require inserting a temperature sensor into the body through a natural opening, like the mouth or ear, without causing excessive discomfort. Invasive methods necessitate inserting the temperature transducer into a deep bodily position, such as the rectum, vagina, esophagus, nasal cavity, bladder, digestive tract, or blood artery (*17*).

The increasing popularity of digital thermometers has led to the removal of mercury thermometers from conventional clinical care due to safety concerns. Digital thermometers, which measure the patient's temperature using a thermistor or thermocouple, have become the go-to thermometry devices. These thermometers are nontoxic, provide precise and easy-to-use measurements that can be taken orally, rectally, or under the arm, and signals can be easily digitized (*9*). They are frequently used in hospitals, clinics, and homes for self-monitoring. Additionally, resistance temperature detectors are another type of digital thermometer used in laboratories for calibrating thermistors and thermocouples (platinum resistance thermometers) (*24*). Thermocouples are highly sensitive to temperature fluctuations and consist of two distinct metal wires linked at one end. A voltage difference between the two wire ends is generated by the metal wire pairs, and the voltage increases with the temperature. This is known as the Seebeck effect (*29*), which allows thermocouples to be used for temperature measurement. However, the accuracy of thermocouples can be affected by the materials used, which may corrode over time (*24*). Thermometry methods, which include the use of thermocouples, typically measure the surface or macroscopic temperature of objects. These methods can be invasive and require a contacting probe, leading to disadvantages such as sensor mismatch, indirect measurements, and a lack of detailed temperature information (*30*). Thermistors, on the other hand, work differently than thermocouples. They are solid semiconductor devices with resistance that varies with temperature depending on the materials used (*24*). Thermistors can exhibit either positive or negative temperature coefficients. In the case of a thermistor with a negative temperature coefficient (NTC), the resistance decreases as the temperature of the material increases. Thermistors with a positive temperature coefficient (PTC) exhibit the opposite behavior. Both types of thermistors exhibit nonlinearity, which poses a challenge for temperature indication. Thermistors with NTC properties are commonly employed for temperature measurements. Thermistors with PTC properties can be used as temperature sensors, but they are also commonly employed as protective devices to limit electric currents when the system exceeds certain temperature thresholds (*31*).

Conventional contact thermometers, such as the traditional mercury and bimetallic thermometers, pyrometers (*5*), thermocouples, and thermistors, are not suitable for temperature measurements of fast-moving objects or on scales less than 10 μm due to the contact nature of such readings (*27*). Although thermocouples and thermistors dominate the market, these traditional contact thermometers rely on an electrical link, which limits their applicability in locations with strong electromagnetic noise and sparks (*27*). These limitations can impact the accuracy and safety of temperature measurements (*27*). Thermometry techniques must advance in order to accurately measure temperature in different applications, such as biomedical research and healthcare.

Optical sensors are among the different sensing technologies that seem to be genuine substitutes for electronic ones because of their intrinsic qualities, which in certain situations are more beneficial, such as contactless, large-scale measurements, faster response times, and immunity to electromagnetic fields (*32*). As a result, it is critical to investigate optical temperature sensing. The first optical temperature sensors were infrared (NIR) thermometers, which detect infrared radiation generated by an object to measure the temperature of the patient's skin, as opposed to contact-based sensors, which require contact with the patient's body to take their temperature. Because of their ease of use and non-invasive nature, they are extensively employed in healthcare settings (*33*). These NIR thermometers are especially useful in medical settings where direct contact with thermocouples is impractical or prohibited. They allow for rapid temperature recording, making them popular due to their high precision without the need for physical contact. Despite these advantages, NIR thermometers have poor spatial resolution, and their reading accuracy is heavily dependent on the

characteristics of the subject under study. Furthermore, accurate calibration is required because NIR thermometry is limited to measuring temperature distribution on object surfaces and cannot provide absolute temperature values. Neverthless, suggested for use in thermometry are now other optical techniques including examples such as thermoreflectance, absorption, Raman spetroscopy, magnetic resonance imaging thermometry, and luminescent techniques (*33*). To find out more about the advantages and disadvantages of this and other optical techniques, see for instance the **Brites et al.** work (*34*). Among non-invasive spectroscopic methods for determining temperature, luminescence has attracted the most attention (*32*). Additionally, temperature from physiological processes in vivo, such as heat generation, heat transmission, and related thermodynamic phenomena, varies at the micro/nanoscale level. As a result, there is a considerable demand for the development of nanothermometry techniques that achieve non-invasive temperature monitoring in vivo with high precision and spatial resolution, which is particularly important for living system process analysis and biomedical applications (*30*). Luminescent micro and nanothermometers have gained popularity as microelectronics, optoelectronics, photonics, nanomedicine, diagnosis, microfluidics, and other sectors have advanced, owing to their high spatial resolution, high sensitivity, wide usable temperature range, and high measurement precision (*35*).

In addition, temperature probes are also classified as primary or secondary thermometers according to their calibration relationships. While thermodynamic laws and quantities are used to determine temperature, the thermometer is considered primary (*35*). Primary thermometers are often inconvenient due to poor reproducibility, slow response time, and difficult operation. Examples of primary luminescent thermometers are extremely scarce (*36*). If the temperature is determined by comparing it to a reference thermal probe, a calibration procedure is required, and the thermometer is classified as secondary. When knowledge of a measurable physical quantity is insufficient to calculate temperature from an equation of state that relates temperature to other measurable physical quantities, the thermometer is referred to as an external temperature reference, also known as secondary (*35*). Secondary thermometers use known reference values, such as triple points of gases and liquids or melting points of metals, to determine the dependence of an observable on temperature changes. Calibration can be non-trivial, so this is an important consideration. Some secondary nanothermometers utilize the direct correlation between temperature changes and variations in photoluminescence intensity. Using a precalibrated nanothermometer in an environment that absorbs or scatters light at its operating wavelengths may result in inaccurate temperature readings. This is a significant limitation of many proposed all-optical nanothermometry techniques (*36*).

In the field of photonics, luminescence thermometry emerges as a promising method for remote temperature measurement (*27*),(*34*). Advancements in all optical remote luminescence nanothermometry have the potential to transform bio and nanomedicine by tackling previously inaccessible challenges (*27*). In recent years, luminescence thermometry has enabled real-time thermal sensing in vivo or intracellular in vitro for developing controlled thermal therapies, monitoring brain activity, early tumor detection, in vivo diagnosis of cardiovascular diseases, inflammation detection, mapping temperature-dependent enzyme activity, gene expression, and cell signaling (*37*). Luminescence thermometry offers a comprehensive solution compared to traditional thermometry methods (*37*). It offers high thermal sensitivity ($S_r > 1\%\cdot°C^{-1}$, the definition of S_r will be found in **Section 2.1.1**), fine spatial resolution (10^{-6} m), and fast acquisition times ($< 10^{-3}$ s) (*34*). microelectronics (*39*), microfluidics (*40*) catalysis (*41*), and nanomedicine (*42*). Additionally, luminescent thermometers can operate in harsh environments, such as biological fluids, strong

electromagnetic fields, cryogenic temperatures, and fast-moving objects, without compromising their resolutions (*43*).

The operating principle is simple: use the luminescence properties of materials — such as luminescence intensity, lifetime, or spectral characteristics — to monitor temperature changes (*6*, *36*). The fundamentals of luminescence thermometry will be later discussed and detailed in **Chapter 2.** A self-reference ratiometric thermometer, which measures the intensity ratio of different spectral regions in the emission spectrum, is a commonly used method for determining absolute temperature (*34*). These thermometers produce consistent temperature readings and are unaffected by local intensity fluctuations. However, external factors such as humidity, pressure, and chemical contaminants can all interfere, reducing accuracy and reliability. Research aims to develop robust measurement protocols and explore strategies for enhancing resilience in challenging environments (*36*).

One solution is to use primary luminescent thermometers, which have a well-established state equation, as previously mentioned (*45*). The majority of the cases concern upconversion phenomena, in which the Boltzmann equation describes the thermally coupled levels involved in emission (*36*). Upconversion necessitates NIR laser radiation, which precludes widespread use in mobile sensing and Internet of Things (IoT) due to safety concerns and the need to adjust the smartphone device. There are very few examples of primary thermometers with downshifting and non-coherent low-power excitation sources (*47–49*). Other examples rely on an empirical equation (*50*) that directly correlates a specific measured value to absolute temperature, eliminating the need for calibration. A recent method employs energy-driven luminescence thermometers, which combine experimental and theoretical calculations (*51*). However, circumventing the calibration curve is not always feasible because the physical mechanism underlying the thermal dependence of optical features is frequently complex or unknown from a theoretical standpoint, limiting the application of this strategy.

Another way to improve robustness is to use synchronous and independent temperature readouts or multiparametric approaches to improve sensibility (*51*). These approaches optimize thermal response by combining two or more thermometric parameters. A few examples include luminescent QR (Quick Response) codes (*51*) printed on commercial medical adhesives with multiplexed color and spatial layers, which allow for simultaneous tracking and multiple synchronized temperature readouts. This is accomplished through calculations using density functional theory, intramolecular energy transfer, and a rate equation model (*52*). Another example is improving the performance of luminescence thermometers by combining multiparametric sensing and multiple regression (*49*). In this dissertation, we employ a multiparametric approach, which will be discussed in detail in the **Chapter 4**.

Over the past decade, there has been a high interest in luminescent thermometry technology, leading to overly optimistic reports on potential new nanothermometers (73). Moreover, the scientific community has seen a surge in the number of luminescent nanomaterials proposed as luminescent thermometers with potential applications in biomedicine (*53*). To be used in a luminescent nanothermometer, the phosphor-generated emissions must meet a number of requirements. These requirements are related to the quality of the emission produced: they should have a high quantum yield and be temperature dependent (*43*). Therefore, many materials have been investigated as potential temperature probes for luminescence thermometry, with temperatures ranging from room to high (20-60°C) (*37*). Fluorescent proteins, nanogels, polymers, organic-inorganic hybrids, nanodiamonds, metal-organic frameworks (MOFs), organic dyes, semiconductor quantum dots (QDs), and lanthanide (Ln^{3+}) doped nanomaterials have all been investigated as potential

thermometers (*43*). **Table 1.1** summarizes the advantages and disadvantages of using these materials as luminescence thermometers as well as examples of their respective figures of merit, which show the maximum relative sensitivity values S_m. **Section 2.1.1** will explain how this S_m works.

Although organic dyes are the most commonly used thermal probes, QDs and Ln^{3+}-based materials are gaining popularity due to their improved photostability and relatively high emission quantum yields. Luminescent thermometers based on Ln^{3+} ions with organic ligands are also known as molecular thermometers (*5*). However, the aforementioned nanomaterials' high toxicity, low stability, single mode sensing, poor accuracy, and low average response sensitivity have limited their potential applications (*54*). For example, QDs have good photostability, quantum efficiency, and tunable fluorescence. However, their intrinsic blinking makes them unsuitable for long-term monitoring of single molecules. QDs' toxicity, caused by heavy metals like cadmium, limits their use in biology and the environment. Additionally, the scarcity of precursor elements in nature makes QDs costly (*55*). Furthermore, compared to molecular fluorescent dyes, CDs have bigger excitation spectra and less photobleaching (*56*). The overall trends in thermo-sensing nanomaterials focus on enhancing photostability and thermal resolution while using low-cost and safe materials (*55*). CDs represent a new generation of thermometers that meet these criteria and are suitable for biomedical applications, such as temperature monitoring during hyperthermia treatment (*55*).

Table 1.1 The advantages and limitations of selected molecules and materials used to create luminescent thermometers (adapted from (*43*)) and the maximum relative sensitivity values (S_m) (VIS=visible range; BWs=Biological Windows).

Luminescent centers	**advantages**	**limitations**	**S_m ($\%\cdot°C^{-1}$)**
Fluorescent proteins	-Allow determining intracellular temperature -High intracellular thermal sensitivity	-Time-consuming gene encoding preparation -Advanced microscopy and biology equipment required	2.2 (*57*)
Nanodiamonds	-High thermal sensitivity -Environment-independent emissions	- Operates only in the VIS region, indicating low penetration depth in biological tissues -Low fluorescence efficiency	n.a.*
Organic dyes	-High thermal sensitivity -Easily incorporation within living cells	-Environment-dependent luminescence properties	1.4 (*58*)
Organic-Inorganic Hybrids	-High thermal sensitivity	- Operates only in the VIS region, indicating low penetration depth in biological tissues; - The spectra recorded may be distorted due to the significant absorption of the various components present in them.	7.2 (*58*)

Table 1.1 Continued...

Luminescent centers	advantages	limitations	S_m ($\%\cdot°C^{-1}$)
Nanogels	-Hight thermal resolution of 0.29 - 0.50 °C over the range of 27 - 33 °C	-Operation restricted to 25 °C - 65 °C	n.a.
Ln^{3+} doped materials	-Photochemically/thermally stable -No phototoxicity/photobleaching; -High quantum yield -Emissions within the BWs; -Excited with NIR light -Emissions can be environment-independent	-Low absorption cross section of f-f transitions	2.3 (*58*)
MOFs	-Tunable luminescence -High thermal sensitivity and thermal resolution	-High toxicity -Unstable in physiological environments	1.2 (*59*)
QDs	-Size-tunable luminescence properties -High quantum yield -High photostability	-Photobleaching -Environment-dependent luminescence properties -May induce changes in genes	1.3 (*58*)

*n.a.=not available

CDs have attracted significant attention in a variety of research domains due to their exceptional properties, which include strong fluorescence, resistance to photobleaching, chemical stability, low precursor cost, low toxicity, and biocompatibility (*60*). Recent research has demonstrated the thermal-sensing capabilities of certain CDs, making them viable alternatives to other nanomaterial-based thermometers (*61*). For example, CDs have advantages over the usually used semiconductor QDs in terms of programmable photoluminescence, simple functionalization, low toxicity, superior biocompatibility, and the absence of blinking (*61*). These luminescent-based thermometers show promise for applications in nanocavity temperature sensing and thermal mapping, providing insights into a more complete understanding of biological processes (*60*). Only a few papers currently use CDs as temperature probes.

A search of the Scopus platform using search terms such as “Carbon Dots”, “thermometry, or thermometer, or thermometric”, and “luminescent, or luminescence, or emission” in the title, abstract, and keywords yields only 37 papers since 2015, as shown in **Figure 1.3-a**. **Figure 1.3-b** presents a global map illustrating the distribution of these publications in various countries, highlighting the worldwide involvement and contributions to this field of study. Notably, this search ignores the pioneering works by ***Yu et al***. (*62*), which deviated from the specific terminology by using "temperature-dependent" rather than “thermometry” and its derivatives. CDs appear as good candidates (*63*), combining stable luminescent properties across a wide temperature range while being sustainable and compatible with various measurement environments. The idea of using CDs as smart materials is currently gaining traction in material and analytical sciences. A material is said

to be "smart" when it responds to a major external physical or chemical stimuli such as light, temperature, pH, solvent, stress, and electric and magnetic fields (*64*).

Leveraging its low toxicity, stability, and hydrophilicity, in this thesis I selected phosphorescent CDs easily excited under low-power excitation sources like light emitting diodes (LEDs) or smartphone flashlights to design smart e-tags for thermal sensing. Furthermore, the phosphoresce will provide additional thermometric parameters improving thermal sensing robustness.

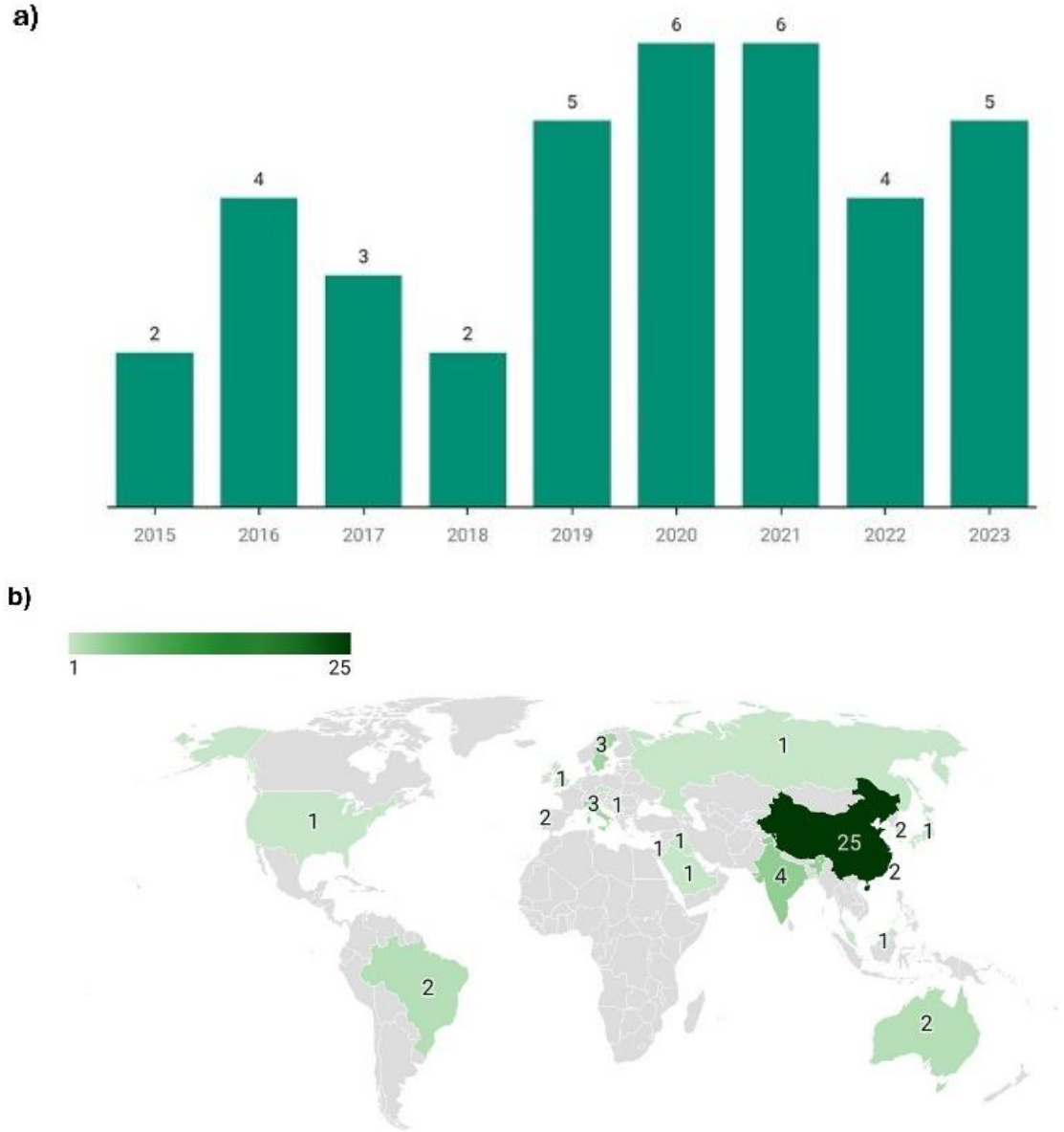

Figure 1.3 Literature search in the Scopus database for the terms "*Carbon Dots*", "*thermometry*, or *thermometer,* or *thermometric*", and "*luminescent, or luminescence, or emission*" in the title, abstract, and keywords. a) Histogram of the number of papers per year. b) World map representing the distribution of the number of papers per country.

Since the onset of the COVID-19 pandemic, non-contact or remote temperature screening techniques have been extensively employed in densely populated areas such as airports, markets, stations, and hospitals. The pandemic has emphasized the necessity for prompt and precise fever detection to reduce the transmission of the virus. Consequently, there has been a rise in the need for temperature measurement devices that do not require physical contact (*22*). Although the CD-based luminescent thermometers processed as smart e-tags discussed further in this dissertation require physical contact with the object being measured, based on the zeroth law of thermodynamics, temperature changes can be remotely monitored and non-invasively using the luminescent thermometry method (*65*). This can be achieved by measuring alterations in the luminescent properties of the probe, either with a portable spectrometer or, for more accessible and practical applications, using a smartphone, as will be shown in **Chapter 4**. This technique offers several advantages, including high-resolution temperature measurement at the cellular level. It enables the mapping of temperature gradients within the intracellular environment of a cancer cell, for instance (*12*).

To better understand the rationale behind integrating CDs into smart e-tags, it is essential to delve into the concept of the IoT. A growing number of physical objects are being connected to the Internet at an unprecedented rate, bringing the IoT concept to life (*66*). Originally conceived in 1999, IoT has evolved significantly, incorporating a wide range of emerging trends, components, and definitions that have been extensively researched and debated over the last decade. What was once a future concept has now become a reality (*5*). IoT enables physical items to see, hear, think, and perform tasks by allowing them to "talk" to one another, share information, and coordinate decisions (*66*). The number of IoT smart objects deployed globally is estimated to reach 212 billion by the end of 2020 (*66*). By leveraging technologies such as ubiquitous and pervasive computing, embedded devices, communication technologies, sensor networks, Internet protocols, and applications, IoT transforms traditional items into objects (*66*). Its ubiquitous impact spans multiple areas such as security systems, environmental monitoring, multimedia, logistics and management, retail, public sector, transportation, smart cities, industry 4.0, and healthcare 4.0, affecting both individuals and organizations (*5*).

In essence, IoT is the fusion of physical, informational, and communication technology to create a network of interconnected things. This network can connect individuals, objects, and services globally. New e-tags are essential in such a notion to identify each node in the network (*5*). Smart e-tags for real-time sensing and establishing human-to-human, human-to-machine, and machine-to-machine communication are a growing market driven by applications such as Industry 4.0, Smart Cities, and Smart and Connected Communities (*67*). Smart e-tags are crucial for authentication, trackability, and counterfeiting detection. They should be trustworthy, ensuring the integrity, validity, and preservation of information for items in circulation or during transactions (*67*). However, smart e-tags go beyond identification and are able to detect and react to the surrounding environment and be embedded with sensors (*68*). Smart e-tags that combine identification and sensors will make items intelligent, and those accessible via a smartphone will stand out as the most viable strategy for widespread adoption in this context (*5*). Sensors play an important role in the ever-expanding domain of the IoT in recording and conveying vital information enhancing our understanding of network dynamics and environmental conditions, and enabling comprehensive monitoring across various parameters (*5*),(*32*). Among these parameters, temperature is particularly important (*9*) and must be carefully monitored, as mentioned earlier. Therefore, it is critical to integrate thermal sensing capabilities into communication networks, expanding our understanding and exploiting its full potential (*69*). Although optical temperature measurement has advantages over

electric temperature measurement as previously stated, its incorporation in the IoT is challenging due to a lack of affordable solutions capable of converting optical into an electrical signal in a cost-effective manner (*69*). Integrating such optical sensors into smartphones offers a promising technique for mobile optical (mOptical) sensing (*69*). In mOptical sensing, smart e-tags readable by smartphones can measure physical parameters such as body temperature while simultaneously connecting to IoT (*7*). These customized tools can significantly enhance personalized healthcare services, making them more effective, secure, and tailored to individual needs. This will benefit e-health and m-health allowing for continuous and real-time monitoring of temperature.

The smart e-tags in this dissertation can be read using smartphones, which aligns perfectly with the expanding IoT ecosystem. This enables seamless integration of thermal sensing capabilities into a vast network of interconnected devices targeting e-Health applications.

1.3. Objectives and Contribution

The primary goal of this dissertation is to create and improve the robustness of luminescent thermometers for real-time applications, using the seamlessly interface with smartphones to support e-health initiatives, allowing for continuous and user-friendly temperature monitoring. To accomplish it, the following goals were defined:

- processing of and characterization of physical mixtures of CDs e-tags made from rhodamine B and dibenzoylmethane;
- investigate the luminescent characteristics of e-tags, their dependence on the temperature (T) and time delay (t), towards the development of a novel ratiometric parameter, $\Delta(T,t)$, deviating from traditional ratiometric thermometers;
- develop methodologies for enhanced thermometry performance;
- exploring CDs' sensitivity to smartphone LED flashlight to ensure smartphone use.
- explore the emission mechanism based on thermally activated delayed phosphorescence (TADP).

1.4. Dissertation Organization

The current dissertation is divided into five chapters. The first one focuses on motivation, framework/state of the art, and goals. The second chapter is devoted to the foundations and background that underpin this dissertation. Chapter three covers the synthesis and characterization of luminescent e-tags. The fourth chapter presents the core results of the dissertation, detailing the optimal thermometric parameters for the luminescent thermometers developed. The final chapter contains the conclusions as well as proposals for future work.

Chapter 2. Fundaments and Background

This chapter focuses on the fundamental principles and background information that underpin the research conducted in this dissertation. This chapter is subdivided into multiple crucial sections. **Subchapter 2.1** explores the fundamental principles of luminescence thermometry and its use in measuring temperature. It explains the mechanisms that allow luminescent materials to work as temperature probes and provides a thorough overview of its principles and historical progression. **Section 2.1.1** provides an overview of traditional sensing methods that rely on luminescence, discussing their specific advantages and limitations. **Section 2.1.2** delves into the topic of multiparametric thermometers, examining the benefits of integrating multiple luminescent parameters to improve the precision and dependability of measurements. **Section 2.1.3** explores the growing practice of mobile sensing, specifically the utilization of smartphones for luminescence thermometry. It discusses the difficulties and advancements related to this method. Every section consists of thorough evaluations of current research, emphasizing notable progress and pinpointing potential avenues for future investigation. This chapter establishes the foundation for the practical and research-oriented material that will be presented in the following chapters.

2.1. Luminescence Thermometry

Optical thermometry methods are used for non-contact measurements and temperature visualization (*70*). Since the beginning of the twenty-first century, there has been a renewed interest in optical thermometry (*71*). Among these techniques, luminescence thermometry is a simple and noninvasive approach for measuring temperature by analyzing the luminescent properties of materials. This method relies on the fact that the intensity, wavelength, and lifetime of luminescence emitted by certain materials change with temperature (*35*).

Luminescence is the emission of light from an excited electronic state of a specific substance, such as a luminescent material, molecule, or ion. This substance is often contained within a matrix or host material. In some cases, a sensitizer may be used to enhance the absorption of light and facilitate energy transfer to the activator. In other cases, the material may only consist of an activator implanted in the host without a sensitizer. By doping the host with modest concentrations of foreign ions, including activators and sensitizers, the typical luminescence attributes of a specific chemical can be achieved in the host (*43*). When an activator is inserted into a host lattice, it produces an emitting center that can be activated to generate light. A sensitizer integrated into a host lattice is capable of more efficiently absorbing energy from the excitation source and transmitting it to a neighbor activator, which will eventually generate luminescence. Based on the duration of emission, luminescence can be classified into two main types: fluorescence and phosphorescence. Fluorescence is a rapid emission process involving a spin-allowed transition between the excited and ground state, where light is emitted almost immediately after absorption of radiation and ceases promptly once the excitation source is removed (*72*). The lifetime of a fluorescence emission can be in the order of nanoseconds for CDs (*73*). In contrast, phosphorescence is characterized by a delayed emission of light that continues for a longer period after the excitation source is removed. Because the emission rates are slow, phosphorescence lifetimes range from milliseconds to seconds. After being exposed to light, the phosphorescence substances glow for several minutes before gradually returning to the ground state (*72*). This is due to the involvement of spin-forbidden transitions that delay the release of energy. Solids that exhibit luminescence are commonly known as phosphors (*74*).

When subjected to heat, the phosphor's luminescence characteristics may vary (*43*). Temperature evolution can be remotely determined using various types of molecular species, nanomaterials, or bulk materials by measuring the changes in the phosphor's luminescent properties (*65*). Exploring how these features change, with the ultimate purpose of calculating the phosphor's temperature, gives rise to luminescence thermometry (*43*). **Figure 2.1** shows a generic schematic representation of the essential processes of luminescence thermometry. For the sake of simplicity, a single-center emission phosphor is depicted, with the intensity of the emissions changing as the temperature rises.

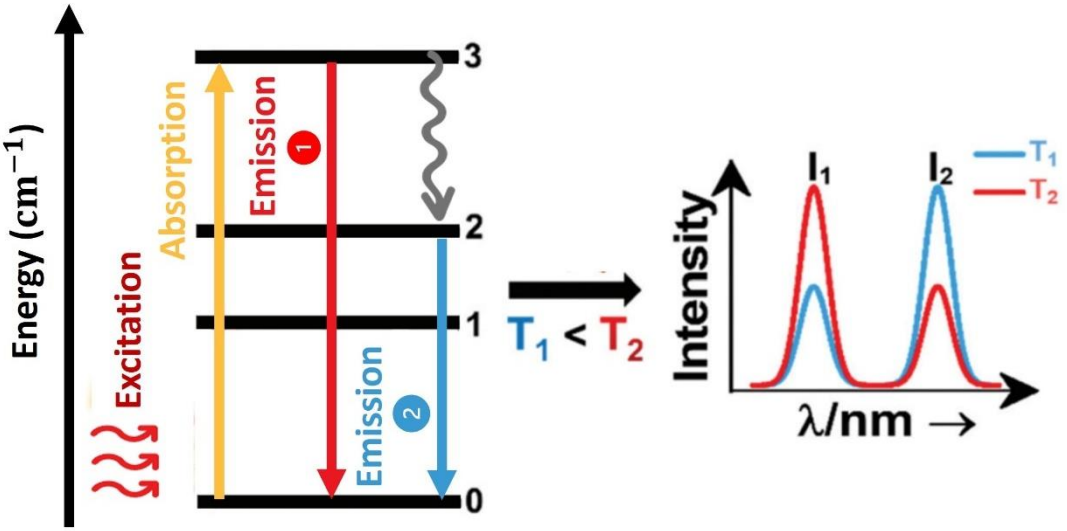

Figure 2.1 Fundamental operating principle of luminescence thermometry evidenced by the change in the intensity of the emissions as temperature increases. Adapted from (*43*).

Figure 2.1 depicts how an energy source excites a phosphor from the ground state (indicated as 0) to an excited state (indicated as 3), from which it decays back to an intermediate or ground state via light emission or energy release via non-radiative processes, in accordance with the principle of energy conservation. The decay could occur directly from the excited state (3) to the ground state (0) via a radiative relaxation process, producing an emission line (labeled as "Emission 1" with intensity I_1), or via a non-radiative relaxation process (shown with a gray wavy arrow) via a lower intermediate excited level (either 2 or 1). A second radiative relaxation process at a lower level or to the ground state can result in the formation of a second emission line (labeled "Emission 2" with intensity I_2).

Luminescence thermometry, dating back to the 1930s, originated with Neubert's method of using phosphor luminescence extinction by infrared radiation for temperature measurement (*75*). This concept was first applied to $Zn_{1-x}Cd_xS$ in 1949, leading to applications in aeronautics and medicine during the 1950s and 1960s. Interest waned until the 1990s, with only about 10 publications per year (**Figure 2.2-a**), despite notable developments in thermographic phosphors for thermal imaging, integrated circuits, fiber tip thermometry, and upconversion laser cooling. A breakthrough occurred around 2000 with the use of luminescent molecules and nanoparticles doped with transition metal and lanthanide ions for microscale temperature measurement. From 2007 to 2012, interest surged, particularly in micro and nanoelectronics, fluidics, photonics, and nanomedicine, with a significant increase in publications (approximately, 80 publications per year, **Figure 2.2-a**) and exponential growth in citations from 500 to 1000 (**Figure 2.2-b**). The first reviews appeared during this period, covering Ln^{3+}-doped glasses, nanoscale thermometry, fluorescent chemical sensors,

inorganic phosphors for extreme temperatures, and various types of micro and nanothermometers. Up to 2009, research was primarily focused on high-temperature thermographic phosphors. Since then, the number of publications and citations in luminescence (nano)thermometry has grown tremendously, now representing about 4% of total publications and citations related to luminescence (**Figure 2.2-c,d**). It is worth noting that these figures have nearly doubled in the last five years (*44*). Every year, we see significant advances in luminescence thermometry across multiple scientific and technological domains.

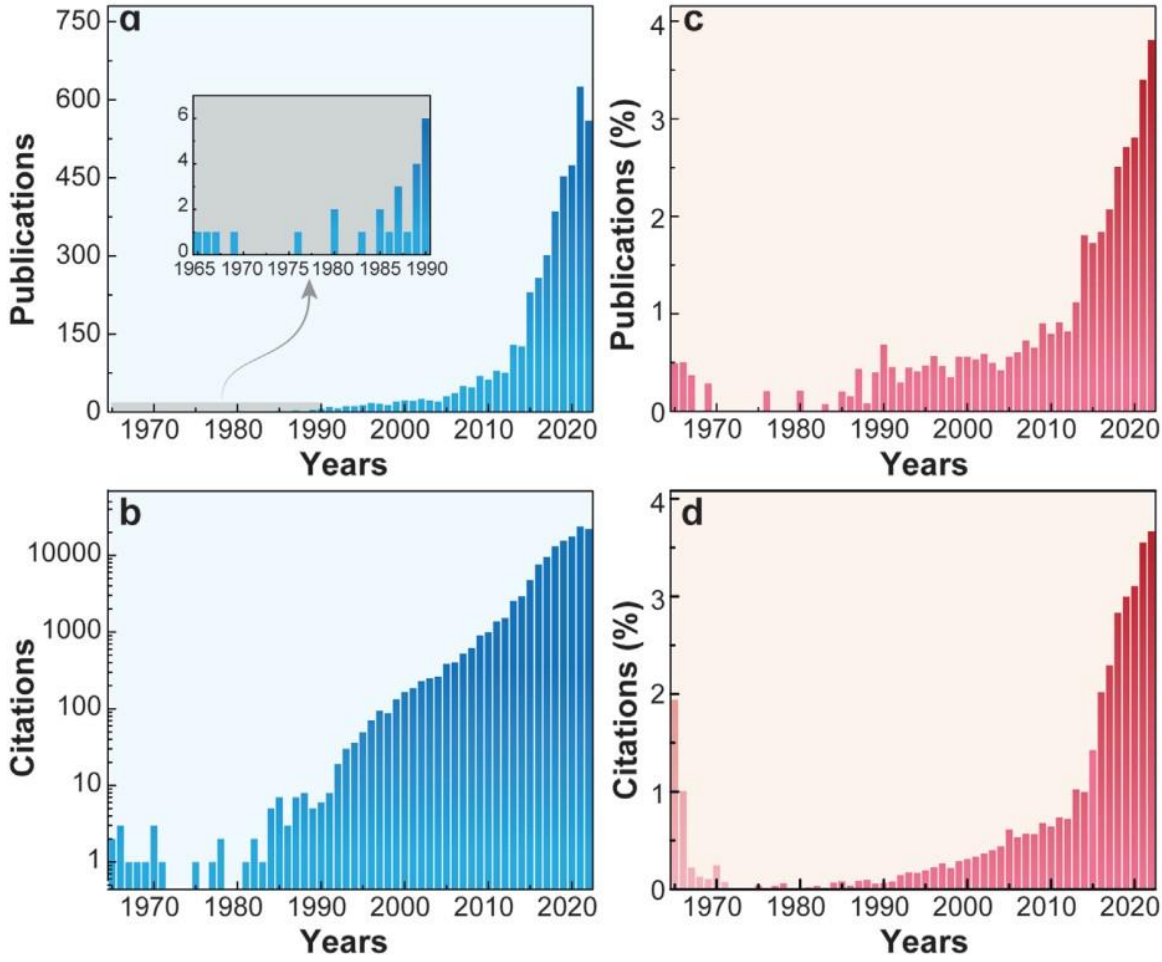

Figure 2.2 a) Number of publications and b) citations of scientific papers using the Web of Science (Clarivate Analytics), principal collection (1900–2022) with the keywords [(luminescence OR fluorescence AND thermometry OR nanothermometry) OR (luminescent OR fluorescent AND thermometer OR nanothermometer) OR (upconversion AND thermometry OR nanothermometry) OR (phosphor thermometry) OR (phosphor temperature-measurements) OR (thermographic phosphors), TOPIC, OR (temperature recording with phosphors), TITLE]. c),d) display the corresponding normalized data to the keywords [luminescent OR luminescence, TOPIC]. Adapted from (*44*).

2.1.1. Conventional sensing

Various methods can be employed to ascertain temperature (temperature readouts) through luminescence, contingent upon the specific use case. Similarly, a wide range of materials can be utilized for the fabrication of a luminescence thermometry probe. The selection primarily depends on the desired working conditions, such as biomedical, nanoscale, or high-temperature engineering, as well as the operating temperature range, precision, complexity, and cost of the thermometer. However, in every instance, the fundamental aspect of the luminescence thermometry application is a measurement. The purpose of a measurement is to ascertain the value of the measurand, which refers to the specific quantity that needs to be determined. In thermometry, the quantity being measured is referred to as the measurand, which specifically refers to the thermodynamic temperature. The process of measurement commences by precisely defining the measurand, selecting the appropriate method of measurement, and establishing the measurement procedure. Luminescence thermometry does not directly measure the temperature value (*75*). Instead, it defines a thermometric parameter $\Delta(T)$, from which the actual temperature is calculated. Absolute intensity, spectral shift, emission branching ratio of two transitions, bandwidth, and luminescence duration of a given excited state are all instances of $\Delta(T)$. The utility of these approaches is determined by the type of luminescence species and the purpose (*37*).

The temperature can be determined easily using the emitted intensity change, I(T), of a single transition, as shown schematically in **Figure 2.3-a**. Unfortunately, the absolute I(T) is influenced by the local phosphor concentration of nanothermometers, the intensity of local illumination, and the transmission properties of tissues. Furthermore, the intensity of many fluorescent thermometers, such as organic molecules, metal complexes, or fluorescent proteins, is influenced by their physical and chemical environments. All of these parameters can change rapidly in living biological samples, resulting in inaccurate absolute thermal readouts (*37*). The luminescence lifetime, $\tau(T)$, (**Figure 2.3-e**) overcomes many of these constraints. The $\tau(T)$ of luminescence thermometers is determined by electronic deexcitation kinetics, regardless of the optical properties of the surrounding medium, nanoparticle concentration, or excitation intensity. Unfortunately, measuring fluorescence lifetimes or imaging in living systems (both in vivo and in vitro) typically requires sophisticated acquisition systems that use either fast detectors or time-gated detection procedures. Despite their obvious advantages, lifetime-based temperature sensors are rarely studied (*37*). Temperature sensing based on bandwidth (**Figure 2.3-d**) or spectral shift (**Figure 2.3-b**) is a desirable option in most cases because it overcomes the limitations of single-intensity thermometers. The spectral overlap between nanothermometer luminescence and the medium extinction coefficient, also known as autofluorescence, is a significant disadvantage. Furthermore, determining the bandwidth or spectral shift requires relatively high-resolution measurements of the entire emission spectra with expensive spectral analyzers, which are even more difficult to quantify in imaging mode (*37*).

Ratiometric-based light thermometers (**Figure 2.3-c**) utilize the intensity ratio of two electronic transitions as the $\Delta(T)$. These thermometers offer the best balance of detection quality, cost, and speed, making them the most promising solution to date. In general, changes in the overall intensity of the excitation source or the local concentration of the thermometers had little impact on the thermal readout, thus addressing the limitations associated with analyzing the emission intensity of a single electronic transition (*37*). This method results in more accurate temperature measurements (34). To convert integrated intensity to temperature, we specify the thermometric parameter, $\Delta(T)$, which is commonly given by the ratio of emission intensities (I_1 and I_2, the integrated intensities of the two transitions (*5*)), as illustrated in *Equation 2.1* (*37*).

$$\Delta(T) = \frac{I_1}{I_2} \tag{2.1}$$

There are some other empirical definitions in the literature, such as *Equation 2.2* (*76*) and *Equation 2.3* (*77*):

$$\Delta(T) = \frac{I_1}{I_1 + I_2} \tag{2.2}$$

$$\Delta(T) = {I_1}^2 - {I_2}^2, \qquad I_1 > I_2 \tag{2.3}$$

However, the integrated intensity ratio of *Equation 2.1* is by far the most frequently used thermometric parameter in comparison with *Equation 2.2* and *Equation 2.3* (*37*). Comparing all the presented methods and considering the number of papers published over the last two decades, ratiometric temperature readout (LIR) between two emission bands is the most popular choice for luminescence thermometry (*71*),(*75*). On the contrary, recent research suggests that previously overlooked experimental artifacts can cause changes in thermometer emission patterns that are not related to temperature. Errors in thermal readings can be caused by factors such as tissue optical properties, thermometer concentration, and excitation intensity (*37*). These findings indicate that even with ratiometric luminescent thermometers, there is a pressing need to have more robust and reliable luminescent thermometers. The design and development of a new generation of luminescent nanothermometers, referred to as "multiparameter nanothermometers", that can provide simultaneous thermal readouts based on various parameters, would enable a definite improvement in thermal noise and reliability in applications like biology and medicine, claim ***Bednarkiewicz et al.*** (*37*). **Section 2.1.2** will delve deeper into the exploration of multiparameter thermometers.

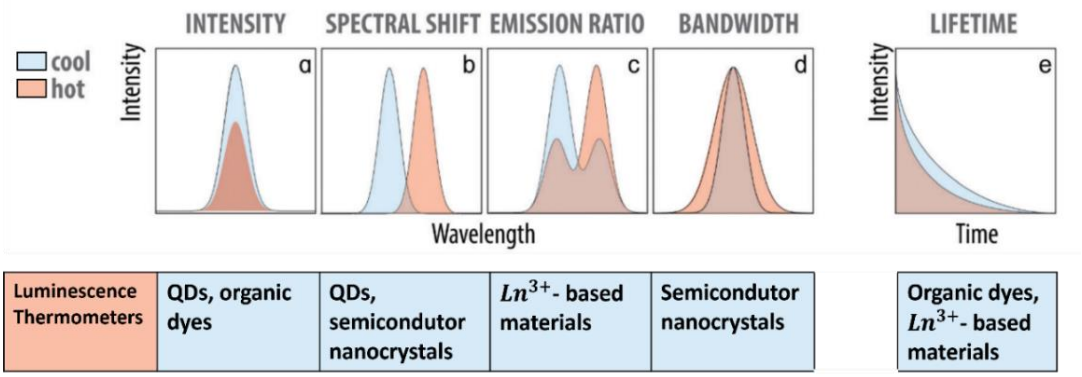

Figure 2.3 Diagram of comparison of the most predominant temperature sensing techniques (a-e). This diagram also lists the emitting species most often used for each technique. Adapted from (*37*).

The quantitative evaluation of any temperature probe's performance is critical for determining its usefulness and comparing various methodologies. The performance of thermometers can be assessed using figures of merit such as relative thermal sensitivity, temperature uncertainty, repeatability and reproducibility and spatiotemporal resolution (*8*).

Thermal sensitivity is the rate at which a thermometric parameter changes in response to changes in temperature (*35*), **Table 2.1**. Thermal sensitivity can be conveyed in two ways: absolute or relative (*43*). Absolute thermal sensitivity (S_a) is denoted as represented in the **Table 2.1** and expressed in units of K^{-1} (*18*). However, comparing the thermal sensitivity of thermometers of various types that operate on different physical principles (e.g., optical, electrical, or mechanical thermometers) or that operate on the same physical principle but use different materials is pointless (*35*). Although it is widely used in the literature, S_a cannot be used to compare the performance of different luminescent thermometers because it is affected by sample characteristics (e.g., absorption and lifetimes) as well as the experimental setup (*5*). To compare the performance of distinct thermometers, regardless of their type or material, the relative thermal sensitivity (S_r) should be used as shown in **Table 2.1** (*35*). Following the proposal of ***Brites et al.*** in 2012 (*58*), this parameter has become broadly adopted as a figure of merit for comparing thermometer performance (*35*). S_r is typically stated as a percent change per degree of temperature change (%. K^{-1}), with S_m representing the maximum value of S_r (occurring at a temperature defined as T_m) (*35*).

The temperature uncertainty (or temperature resolution), δT, is the smallest temperature that the thermometer can resolve, which depends on both the material and the experimental equipment (*8*). Several factors contribute to temperature uncertainty, including the experimental detection setup, acquisition settings, and signal-to-noise ratio (*8*). Typical $\frac{\delta\Delta}{\Delta}$ values for portable detection systems may reach 0.1% at best, implying that typical sensitivities of 0.1-10 %. K^{-1} equate to a temperature uncertainty of 1-0.01 K. When measuring temperature at multiple locations, spatial resolution refers to the shortest distance between points with a temperature difference greater than δT. The spatial resolution (δx) is presented in **Table 2.1** (*43*). The temporal resolution (δt) of a measurement is defined as the shortest time interval between observations with a temperature difference greater than δT, as shown in **Table 2.1** (*43*). The spatial-temporal resolution values obtained with luminescent thermometers were compared to those obtained with other (non-luminescent) non-contact techniques, including thermoreflectance and Raman spectroscopy (*78*). The variation in repeat measurements taken under identical conditions is known as repeatability (R) (*43*). A quantity is considered repeatable if different measurements taken with the same instrument or procedure over a given time yield the same result (*43*). A thermal probe's repeatability is frequently evaluated by cycling the temperature over a predetermined interval, ensuring that each measurement is taken with the probe in thermal equilibrium with the temperature controller (*43*). **Table 2.1** shows the formula used to quantify the repeatability of a thermometer's readout during temperature cycling, where Δ_c is the mean thermometric parameter (extracted from the calibration curve) and Δ_i denotes the measurement value of each thermometric parameter (*43*). A thermometer's reproducibility, on the other hand, refers to the variation of the same measurement performed under different conditions (e.g., different equipment in use, different measuring methods, different observers, etc.) (*35*). Thermal sensitivity and temperature resolution are the most commonly reported performance parameters, while the others are rarely used to determine the performance of a luminescent thermometer, despite their importance in real-world applications (*43*).

Table 2.1 Definitions of luminescence figures of merit.

Figures of Merit	Mathematical Definition
Absolute thermal sensitivity ($\boldsymbol{S_a}$)	$S_a = \frac{\partial \Delta(T)}{\partial T}$
Relative thermal sensitivity ($\boldsymbol{S_r}$)	$S_r = \frac{1}{\Delta(T)}\left\lvert\frac{\partial \Delta(T)}{\partial T}\right\rvert$
Temperature resolution ($\boldsymbol{\delta T}$)	$\delta \mathrm{T} = \frac{1}{S_r}\frac{\delta \Delta}{\Delta}$
Spatial resolution ($\boldsymbol{\delta x}$)	$\delta x_{min} = \frac{\delta \mathrm{T}}{\mathrm{d}T/\mathrm{d}x}$
Temporal resolution ($\boldsymbol{\delta t}$)	$\delta t_{min} = \frac{\delta \mathrm{T}}{\mathrm{d}T/\mathrm{d}t}$
Repeatability (**R**)	$R = 1 - \frac{\max(\lvert\Delta(T)_c - \Delta(T)_i\rvert)}{\Delta(T)}$

2.1.2. Multiparametric Thermometer

From the point of view of thermometric responses, some studies have been using a multiparametric approach to obtain a better response of the thermal sensitivity (*51*, *79*). These approaches involve optimizing the thermal response by utilizing two or more thermometric parameters to measure temperature, leading to enhanced S_r and δT values (*79*). This method was first implemented in the field of luminescence thermometry using multiple linear regression (MLR). MLR evaluates the influence of different independent variables on a single experimental result by incorporating data from various thermometric parameters (*79*). ***Maturi et al.*** have achieved a significant enhancement in the efficiency of multiparametric nanothermometers, surpassing the conventional method by a factor of ten. They have set a new world record for S_r with a value of 50%.K^{-1}, and have achieved competitive δT values below 0.1 K (*79*). The researchers chose enhanced green fluorescent protein (EGFP) and Ag^2S nanocrystals to investigate different photoluminescent properties of the emitting centers, including peak energy, full width at half maximum (FWHM), and the intensity ratio between emission components. These properties can be utilized for thermal sensing in biomedical applications (*79*). The multiparametric analysis is not limited to Ln^{3+} centers. For example, a tenfold increase in S_r is also observed in all-optical nanodiamond thermometry when using the photoluminescence of SiV color centers (*80*). In addition, the technique of MLR was used in Mn^{2+}/Tb^{3+}-codoped Ca_2LaTaO_6 luminescent thermometers. This technique combined the peak energy and FWHM of the Mn^{2+} emission with LIR between the Mn^{2+} and Tb^{3+} transitions. As a result, there was a notable enhancement in the sensitivity to temperature change (from 3.6 to 16% K^{-1}) and the temperature resolution (1×10^{-3} K) (*81*). Based on research demonstrating the advantages of multiparametric thermometry over classical single-parameter methods, as well as its potential to improve the performance of luminescence thermometers (*82*), this dissertation will focus on developing a novel multiparametric thermometer with improved sensitivity.

2.1.3. Mobile sensing

Recent sensor strategies anticipate future designs of compact, lightweight, portable, and low-cost sensor systems. Because of their portability and extensive availability, smartphones have the potential to serve as a platform for the development of next-generation cost-effective hand-held sensors (*75*). Smartphones are now capable of many cutting-edge healthcare applications, including singlemolecule imaging, medical diagnosis, and biosensing, which were previously only possible with bulky devices, thanks to recent developments in high-performance computing, high flexibility, and multiplexed capability. Additionally, smartphones are becoming more affordable and accessible, making m-health technology more popular, especially in resource-limited settings or during pandemics (*83*). Smartphone-based sensor systems have a huge potential subscriber base due to their widespread availability (*75*).

Traditionally, the assessment of luminescence properties for temperature sensing has relied on costly and complex equipment, such as spectrometers or optical interrogators, to capture necessary optical signals, including spectra or decay curves. However, recent research has explored the use of smartphones to measure the luminescence properties such as optical spectra and emission lifetimes for temperature detection (*51*), (*75*). Smartphone-based optical thermometers, or mOptical thermometers, which include luminescence thermometers, have been reported (*84*). ***Pan et al***. measured temperature using a smartphone to observe changes in the TiO_2 thin film reflection spectrum (*85*)**.** ***Zhu*** demonstrated a cost-effective method for recording upconversion emission decays using a smartphone (*86*). ***Araque et al.*** developed a method for measuring gaseous oxygen concentrations in packed foods using a luminescent membrane that detects O_2 and can be read using a smartphone (*87*). ***Ramalho et al.*** developed smart luminescence QR codes that can store information and sense temperature in real-time using a smartphone's charge-coupled device. QR codes made with organic-inorganic hybrids containing europium (Eu^{3+}) and terbium (Tb^{3+}) ions can detect temperature exposure based on the intensity ratio of red and green pixels in a smartphone image (*50*). In these thermometers, smartphones are modified with additional components and used to read thermometric parameters and generate persistent luminescence using white-emitting LEDs coupled to a smartphone's charged coupled device (CCD) camera (*69*). This innovation leveraged the advanced camera and processing capabilities of modern smartphones to offer a more accessible and cost-effective solution for temperature sensing. Several factors have driven the adoption of smartphone-based luminescence thermometry, including ubiquity, portability, high-resolution cameras, and powerful smartphone processors. These devices can record and interpret luminescence signals, analyze the luminescent properties of materials, and convert data into precise temperature readings using specialized apps. Some sources (*88*),(*89*) suggest that smartphones are an important component in the development of mOptical sensors for IoT and may be the principal method for optical temperature sensors because of their processing capability and ability to convert optics into electronics via the CCD camera (*69*). **Figure 2.4** illustrates the thermometric properties utilized in luminescence thermometry and their application in mOptical sensing for IoT. Furthermore, it illustrates that photographs captured with a smartphone of materials that emit light can be utilized to instantly measure the exact temperature, thereby facilitating the extensive adoption of luminescence thermometry (*69*).

Figure 2.4 The diagram illustrates the thermometric properties employed in luminescent thermometry. These properties are utilized in optical sensing for the IoT. Reproduced from (*5*).

Smartphone-based luminescence thermometers can be used to continuously monitor patients' body temperatures, providing a non-invasive and convenient solution (*7*). In terms of performance, ***Ramalho et al.*** compare the S_m (defined in **Section 2.1.1)** of conventional ratiometric luminescence thermometers to the S_m of mOptical thermometers. The findings show that smartphone-based luminescence thermometers achieve S_m values that are comparable to or greater than those of conventional thermometers, demonstrating their potential (**Figure 2.5-a**) (*32*). They also look at the S_r values for primary luminescent thermometers. Notably, only one example uses smartphone-based luminescence thermometry, and it has the highest S_r value among the thermometers tested (**Figure 2.5-b**). This demonstrates the significant potential of smartphone-based approaches in achieving higher sensitivity than traditional methods (*32*). The incorporation of smartphone technology not only provides a convenient and accessible method of temperature measurement, but also improves the overall performance of luminescence thermometers.

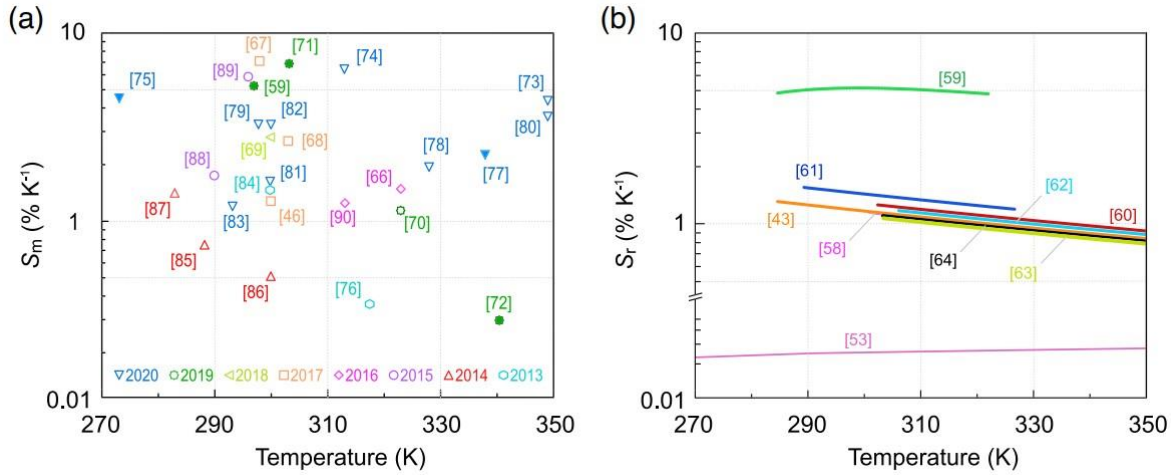

Figure 2.5. a) Values of maximum thermal sensitivity (S_m) for ratiometric luminescent thermometers (hollow symbols) and smartphone-based luminescence thermometers (solid symbols). b) S_r values as function of the temperature for primary luminescent thermometers. Reproduced from (*32*).

Considering what has been said in **Chapters 1 and 2**, one approach to solving the challenges presented is to combine the development of new materials for optical sensing, such as CDs, with the optimization of thermal response using, for example, a multiparametric parameter, and the use of today's widely available hardware (smartphone) to collect and analyze the information that the materials provide, whether to sense temperature or any other physical or chemical parameter. This will allow us to continue moving forward, developing new alternatives to traditional methods and identifying better ways to measure temperature. Taking this into account, my dissertation will discuss the creation of new luminescent thermometers to achieve this goal.

Chapter 3. Production of the luminescent e-tags

This chapter describes the creation of luminescent e-tags, with a focus on the synthesis, characterization, and photoluminescence properties of CDs. The chapter is organized into several sections. **Section 3.1** provides a brief introduction to CDs, highlighting their intriguing properties such as low toxicity, stability, and hydrophilicity, as well as the specific phosphorescent CDs selected for thermal sensing applications. **Section 3.1.1** describes the materials and methods used, including precursor materials and detailed procedures for synthesizing various types of CDs and creating e-tags of various compositions. **Section 3.2** describes structural and morphological characteristics using techniques such as transmission electron microscopy (TEM). Finally, **Section 3.3** investigates the optical features such as UV-visible absorption spectroscopy, steady-state photoluminescence (steady-state emission and excitation spectra), absolute emission quantum yield, the temperature dependence of emission spectra and the time-resolved emission spectra.

3.1. Synthesis of the luminescent e-tags

CDs are intriguing nanoparticles with a size of less than 10 nanometers. They consist of a carbon-based core and exhibit tunable optical properties, which can be adjusted through surface functionalization (*63*). Extensive reviews have been conducted on carbon dots regarding their synthesis, physicochemical properties, and potential applications (*55*). Using its low toxicity, stability, and hydrophilicity, specific phosphorescent CDs were chosen that are easily excited under low-power excitation sources such as LEDs or smartphone flashlights to design smart e-tags for thermal sensing. Through surface functionalization with distinct organic molecules it is possible to tune the photoluminescence features, as described below.

3.1.1. Materials and methods

Dibenzoylmethane (DBM, ABCR), rhodamine B (RhB, Sigma-Aldrich), boric acid (BA, ABCR), ethanol (EtOH, VWR), and sodium hydroxide (NaOH, VWR) were used as received. The molecular structures of DBM, RhB and BA are shown in **Figure 3.1.**

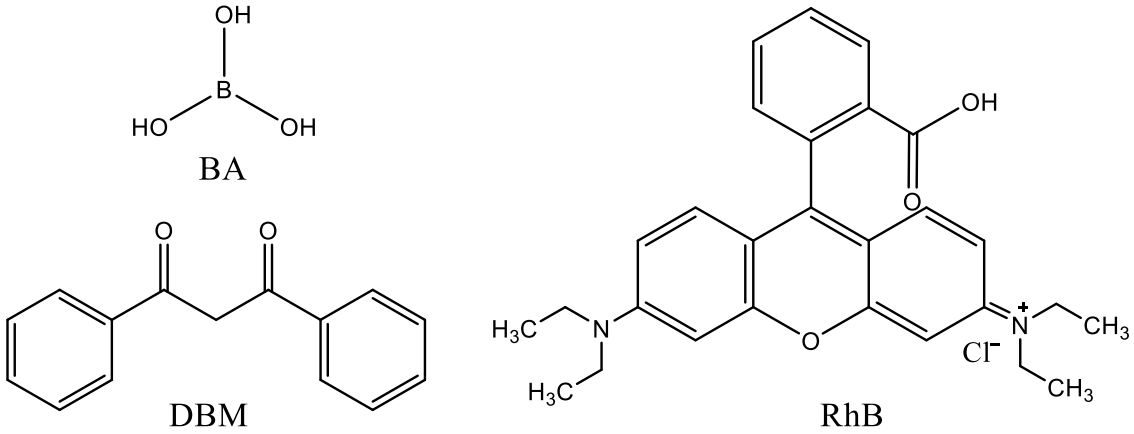

Figure 3.1 Molecular structures of the precursors.

To produce luminescent e-tags, CDs were synthesized using specific precursor materials and methods. The synthesis of the luminescent e-tags was performed in collaboration with Doctor Lianshe Fu, Principal Researcher of the Department of Physics and CICECO – Aveiro Institute of Materials, University of Aveiro. This section details the synthesis procedures for different types of CDs, as well as the preparation of e-tags with varied compositions.

Synthesis of CDs e-tag CD_A: CD_A was synthesized according to literature (*90*). Typically, 10.0 mg of DBM (0.40 mL of DBM in EtOH, 25.0 mg/mL) was mixed with 1.0 g of BA. The mixture was mixed well and calcinated at 225 °C for 15 min, taken out from the oven, and cooled down to room temperature naturally.
Synthesis of CDs RhBCDs: RhBCDs were synthesized according to literature (*91*). Typically, 96 mg of RhB was dissolved in 15 mL of a 0.67 M NaOH solution with ultrasonic treatment. The clear solution was transferred into a poly(tetrafluoroethylene)-lined autoclave (20 mL) and heated at 180 °C for 8 h and cooled down to room temperature naturally. The resulting aqueous solution was diluted to 20 mL with water and named as RhBCDs.
Synthesis of CDs e-tag CD_B: CD_B was synthesized according to literature (*92*, *93*). Typically, 0.25 mL of RhBCDs aqueous solution was mixed with 2.0 g of BA. The solid was ground well and dried at 90 °C to get a dried powder. The powder was calcinated at 235 °C for 15 min, moved out of the oven, and cooled down to room temperature naturally.
Preparation of CDs e-tags CD_{AB}: E-tags CD_{AB} were obtained by mixing CD_A and CD_B in a weight ratio (A:B) of 1:1, 1:4, and 4:1, respectively. These mixtures were ground well, and pellets were made for further characterizations.
Synthesis of undoped sample: For control experiment, 2 g of BA was also calcined at 230 °C for 15 min to obtain the heated BA.

The **Table 3.1** provides a clear overview of the different compositions used for the e-tags, highlighting the proportion of DBM and RhB in each variant. These varied compositions allow for the exploration of different optical and thermal properties in the resulting e-tags.

Table 3.1 Composition of CDs e-tags derived from different precursors

	E-tag name	**DBM**	**RhB**
Pure CDs	CD_A	100%	0%
	CD_B	0%	100%
Mixed CD_{AB}	CD_{11}	50%	50%
	CD_{14}	20%	80%
	CD_{41}	80%	20%

3.2. Structural and morphological characterization

Prior research has thoroughly examined the structures and dimensions of carbon dots produced from DBM (CD_A) and RhB (CD_B) using high-resolution transmission electron microscopy (TEM), X-ray photoelectron spectroscopy to analyze surface compositions, Fourier-Transform Infrared Spectroscopy spectra to clarify the surface functional groups and bonding environment, Raman spectroscopy for component analysis, and X-ray diffraction to evaluate crystallinity and phase composition (*90*). Building upon these foundational insights, TEM images will be presented to showcase the shape and size distribution of the CDs.

3.2.1. Transmission electron microscopy (TEM)

TEM images were taken at the Iberian Nanotechnology Laboratory with a JEOL JEM 2100 (200 kV) microscope. CD_A and CD_B samples were dispersed in water and placed into the analyzing grids (UC-A on holey 400 mesh Cu grids, Ted Pella ref. 01824) by drop-casting, before being dried at room temperature. **Figure 3.2** shows the TEM images of CD_A and CD_B. The presence and structural characterization of CDs in CD_A and CD_B were previously reported in a recent article (*90*). High-resolution TEM images show the presence of CDs with a nearly spherical shape and average diameter sizes of 4 ± 1 and 5±1 nm for CD_A and CD_B, respectively. Fast Fourier Transform analysis of TEM images reveals the presence of highly crystalline structures with a lattice fringe spacing of 0.21 nm, which corresponds to the (100) interplanar spacing of graphene (*94*),(*95*),(*96*).

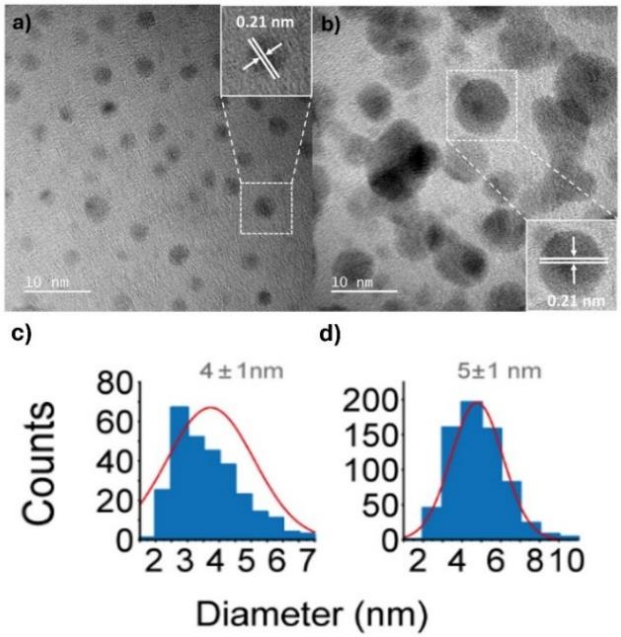

Figure 3.2 High-resolution TEM images of a) CD_A and b) CD_B, and the size distribution of c) CD_A and d) CD_B respectively. Inset images identify individual CDs showing lattice fringes with the corresponding d-spacing determined by Fast Fourier Transform analysis. The line in c) and d) represents the data best fit to a Gaussian function.

3.3. Optical and photoluminescence features

CDs synthesized from DBM (CD_A) and RhB (CD_B) precursors were selected to process mixed e-tags because of their intriguing properties, which include high absolute emission quantum yield (up to 0.52) and phosphorescence emission characterized by long lifetimes activated under low-power excitation (*90*). This rationale for selection of these CDs families makes an easier and more sustainable solution to explore different mixture ratios benefiting from the optical contribution of each component, CD_A and CD_B and add the previously suggested interaction between them that results in an emission spectra that is not only the individual sum of CD_A and CD_B (*90*). In the following sections, the UV-visible absorption spectra was obtained to study the optical properties and electronic transitions of the CDs and the photoluminescence mechanism is described in detail by investigating the emission dependence on different mixture ratios.

3.3.1. UV-visible absorption

The Perkin Elmer Lambada 950 UV/VIS/NIR spectrometer was used to measure UV–visible absorption spectra between 200 to 700 nm with a scan speed of 110 nm/min at room temperature. **Figure 3.3** depicts the UV–visible absorption spectra of BA, CD_A and CD_B. BA absorbs almost no light between 200 and 700 nm. The peaks at 250 nm for CD_A and at 230/275 nm for CD_B are attributed to the π–π* transitions of C=C bonds, while the peak at 350 nm for CD_A and the weak peak at 315 nm for CD_B are attributed to the n–π* transitions of C=O bonds, of the CDs derived from different organic molecules. The broad band in the visible region at 484 nm with a shoulder at 455 nm for CD_B are associated with the absorptions from RhB. These visible absorption bands lead to the fact that these CDs can be excited with a visible light and produce persistent luminescence at room temperature (*90*).

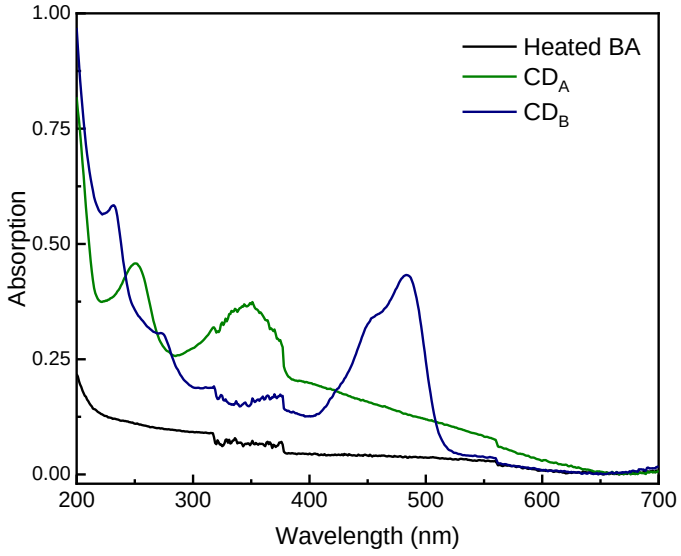

Figure 3.3 UV–visible absorption spectra of Heated BA, CD_A and CD_B. Concentrations: 10 mg/mL aqueous solutions for Heated BA and CD_B and 2.5 mg/mL aqueous solution for CD_A. 1 cm quartz cell was used for all the measurements.

3.3.2. Steady-state spectroscopy: emission and excitation spectra

The photoluminescence spectra were recorded with a modular double-grating excitation spectrofluorimeter equipped with a TRIAX 320 emission monochromator (Fluorolog-3, Horiba Scientific) coupled to an R928 Hamamatsu photomultiplier. The spectra were corrected for the detection and optical spectral response of the spectrofluorometer. The emission quantum yield values were measured at room temperature using a system (C9920-02, Hamamatsu) that included a 150 W xenon lamp coupled to a monochromator for wavelength discrimination, an integrating sphere as the sample chamber, and a multichannel analyzer for signal detection. The method is accurate within 10%. CD_A presents a broad excitation band ranging from 240 to 420 nm (**Figure 3.4**).

Upon excitation with different wavelengths, CD_A shows excitation-independent emission with the maximum emission wavelength of 443 nm, indicating that CD_A has homogeneous surface states. The emission band extends from around 400 to more than 600 nm, generating a bluish color with CIE of (0.21,0.25) (**Figure 3.6**) (*90*).

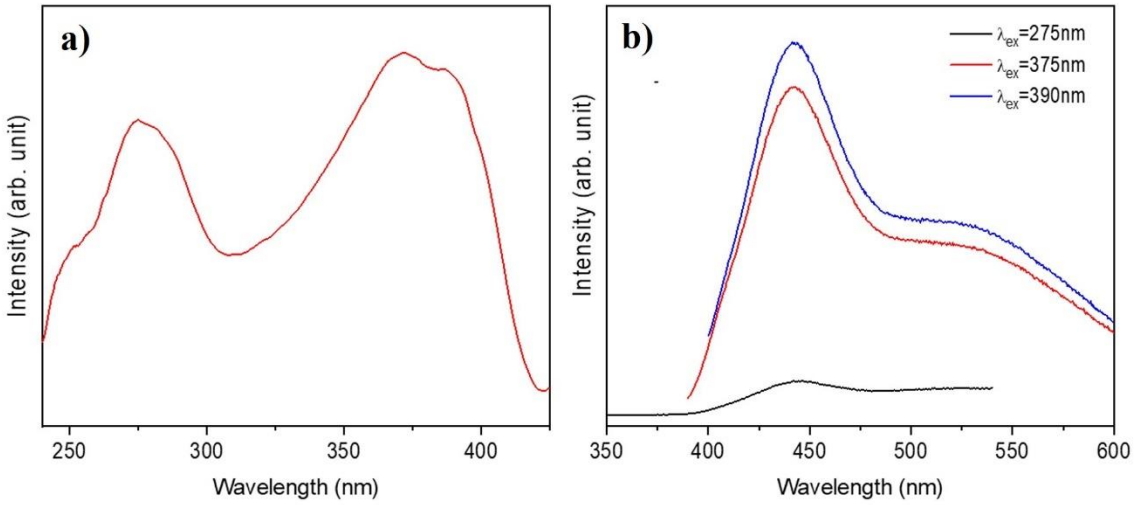

Figure 3.4 a) Excitation and b) emission spectra monitored at 443 nm and excited between 275 and 390 nm, respectively for CD_A

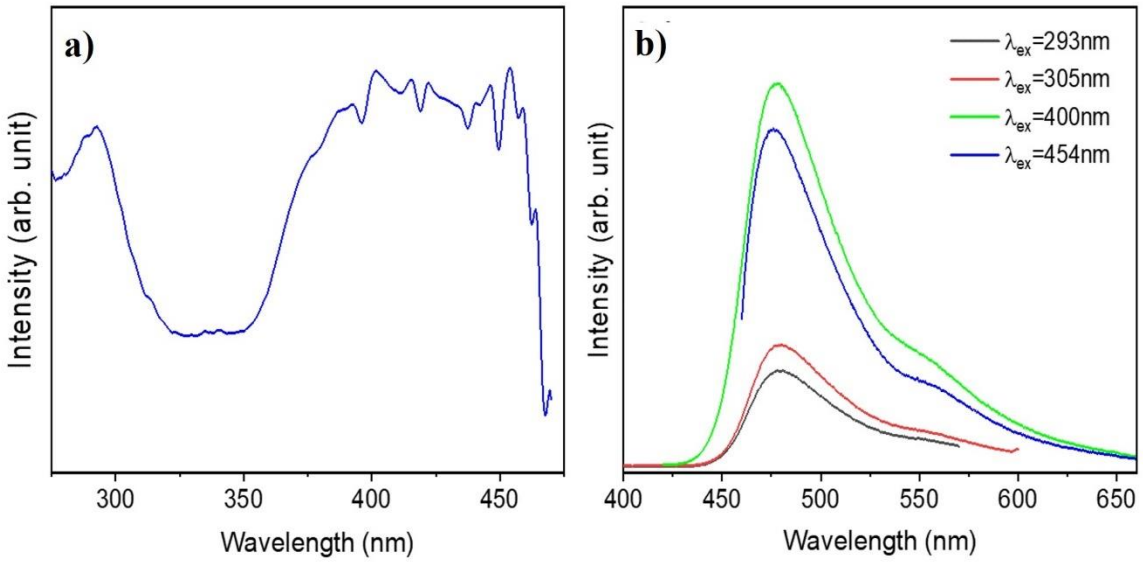

Figure 3.5 a) Excitation and b) emission spectra monitored at 479 nm and excited between 293 and 454 nm, respectively for CD_B.

Compared to CD_A, CD_B also shows a broad excitation band, that extends to the visible spectral region. Upon excitation with either UV radiation (293, 305, and 400 nm) or visible light (454 nm), CD_B also exhibits excitation-independent emission with the maximum emission wavelength of 479 nm (**Figure 3.5**), a luminescence feature similar to CD_A (**Figure 3.4**). The emission band spans from 425 to 650 nm and has a cyan color with CIE of (0.20,0.35) (**Figure 3.6**).

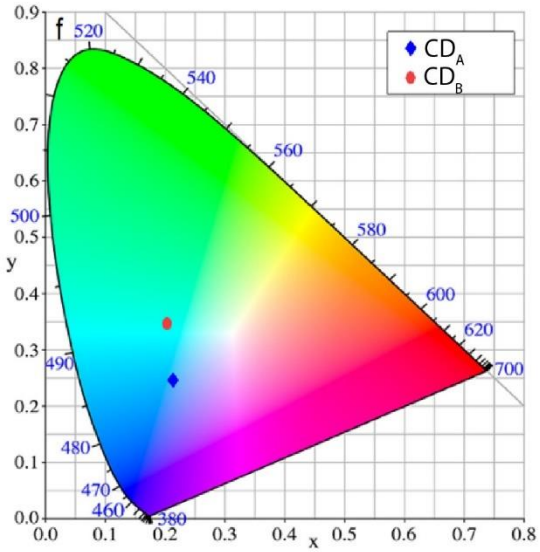

Figure 3.6 CIE chromaticity diagram of the emission spectra of CD_A and CD_B.

Considering the mixed e-tags, the emission spectra of CD_{41} (**Figure 3.7-a**) show broad bands across the visible spectral region, that vary in intensity depending on excitation energy (**Figure 3.7-b**). The emission color is perceptible to the naked eye under UV LED or flashlight illumination (**Figure 3.7-c**), displaying a blue color with CIE of (0.18, 0.20) in the first case (**Figure 3.7-d**). When

the excitation is turned off, a delayed emission occurs (**Figure 3.7-c**), which will be further explained in the **Section 3.3.3**.

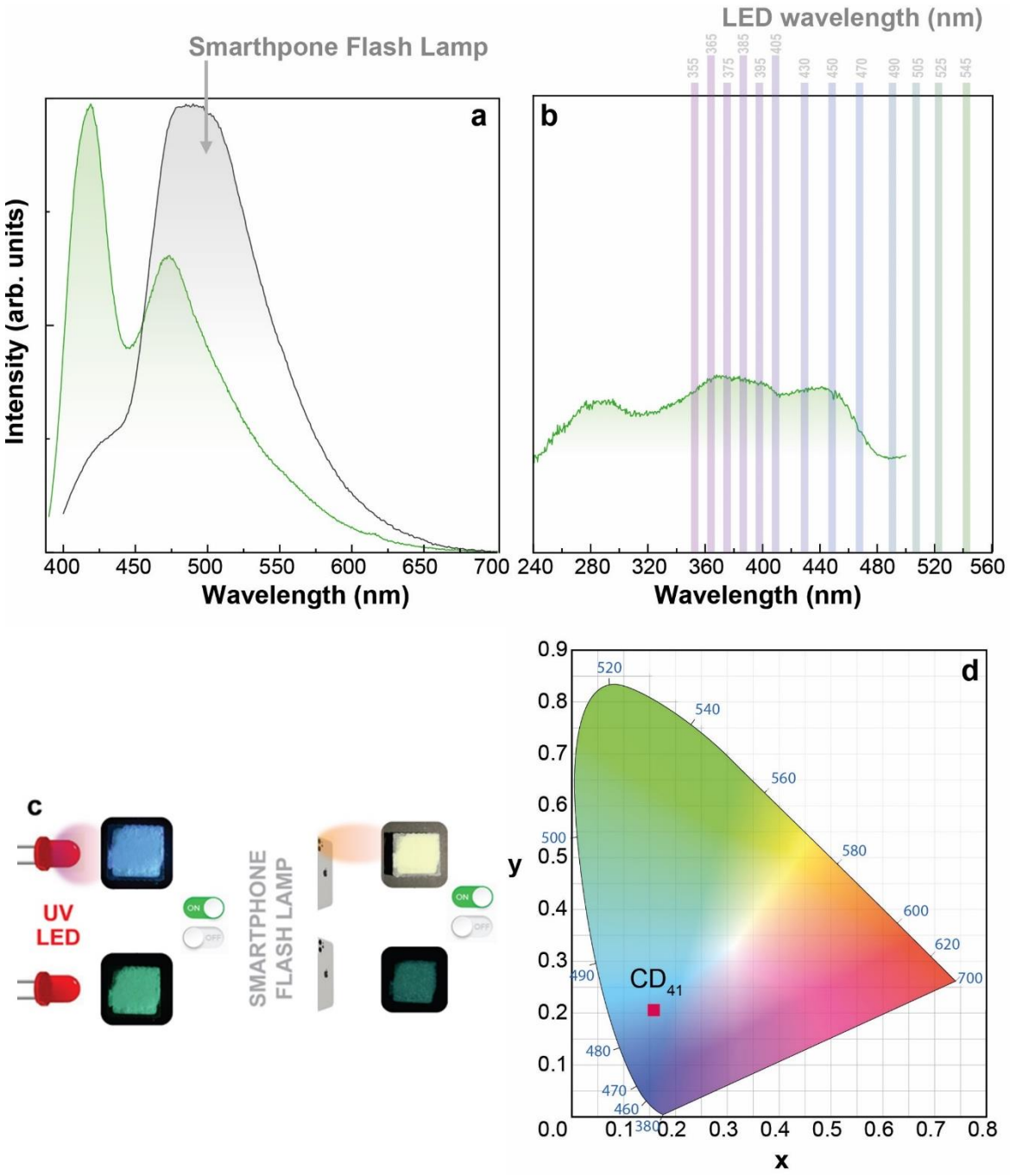

Figure 3.7 a) Emission spectra excited at 370 nm of CD_{41} (the grey shadow is the flash lamp emission spectrum). b), Excitation spectra monitored at 520 nm of e-tag CD_{41}, c) Photographs (1×1 cm^2) under UV or smartphone flash lamp of e-tag CD_{41} and d) CIE chromaticity diagram.

3.3.2.1. Absolute emission quantum yield

The quantum yield (QY) values were measured for CD_A and CD_B in powder under various excitation wavelengths and summarized in **Table 3.2**. CD_A and CD_B exhibit strong emission with high QY value of 0.35±0.03, unlike most of CDs in solid state that experience the aggregation induced quenching. It should be noted that the mixed e-tags CD_{AB} have even bigger QY values (*90*).

Table 3.2 Absolute emission quantum yield (QY) for samples CD_A, CD_B and CD_{41} excited at different wavelengths (λ_{ex}).

CDs	**λ_{ex} (nm)**	**QY**	**CDs**	**λ_{ex} (nm)**	**QY**	**CDs**	**λ_{ex} (nm)**	**QY**
CD_A	275	0.19±0.02	CD_B	293	0.23±0.02	CD_{41}	375	0.52±0.05
	375	0.33±0.03		305	0.26±0.03		405	0.46±0.05
	390	0.35±0.03		400	0.35±0.03		430	0.39±0.04
				454	0.35±0.03		470	0.28±0.03
							490	0.20±0.02

3.3.3. Emission spectra as a function of temperature and time

Both pure CDs and mixed CDs exhibit phosphorescence emission. The prolonged emission has been attributed to the presence of the B_2O_3 host, as reported in the literature (*90*). **Figure 3.8-c,d** (pure CDs) and **Figure 3.10-d-f** (mixed CDs) demonstrate spectral changes after the excitation is turned off.

The CD_A emission spectra show a phosphorescence component centered at ~510 nm and a fluorescence emission centered at ~440 nm (**Figure 3.8-c**). The CD_B spectra reveal two phosphorescence components, ~475 nm and ~550 nm, respectively (**Figure 3.8-d)**. In particular, CD_B exhibits an aggregation-induced state (AIS) (*97–99*), which experiences a population increase due to TADP (*100*) process, as represented schematically in a Perrin-Jablonski diagram (**Figure 3.9-b**) and evident with the increase in the emission intensity, I_B^1, with temperature (inset **Figure 3.8-b**). The TADP is distinguished by delayed emission following the cessation of an external excitation source, such as light (or electricity). This delayed emission occurs when the excited triplet state transitions returns to the ground state via a thermally activated process. In TADP materials, the excited triplet states have longer lifetimes than traditional thermally activated delayed fluorescence (TADF),(*101*, *102*) allowing for delayed emission. In contrast, CD_A does not exhibit either the AIS phenomenon (**Figures 3.8-a** and **3.9-a**) or the TADP effect, at least within the spectral region of interest. Instead, it appears to attenuate the AIS and the TADP effects exhibited by CD_B, thereby affecting in a positive way the thermometric performance. This combined effect (AIS and TADP) on CD_B results in lower values of S_r, as detailed below.

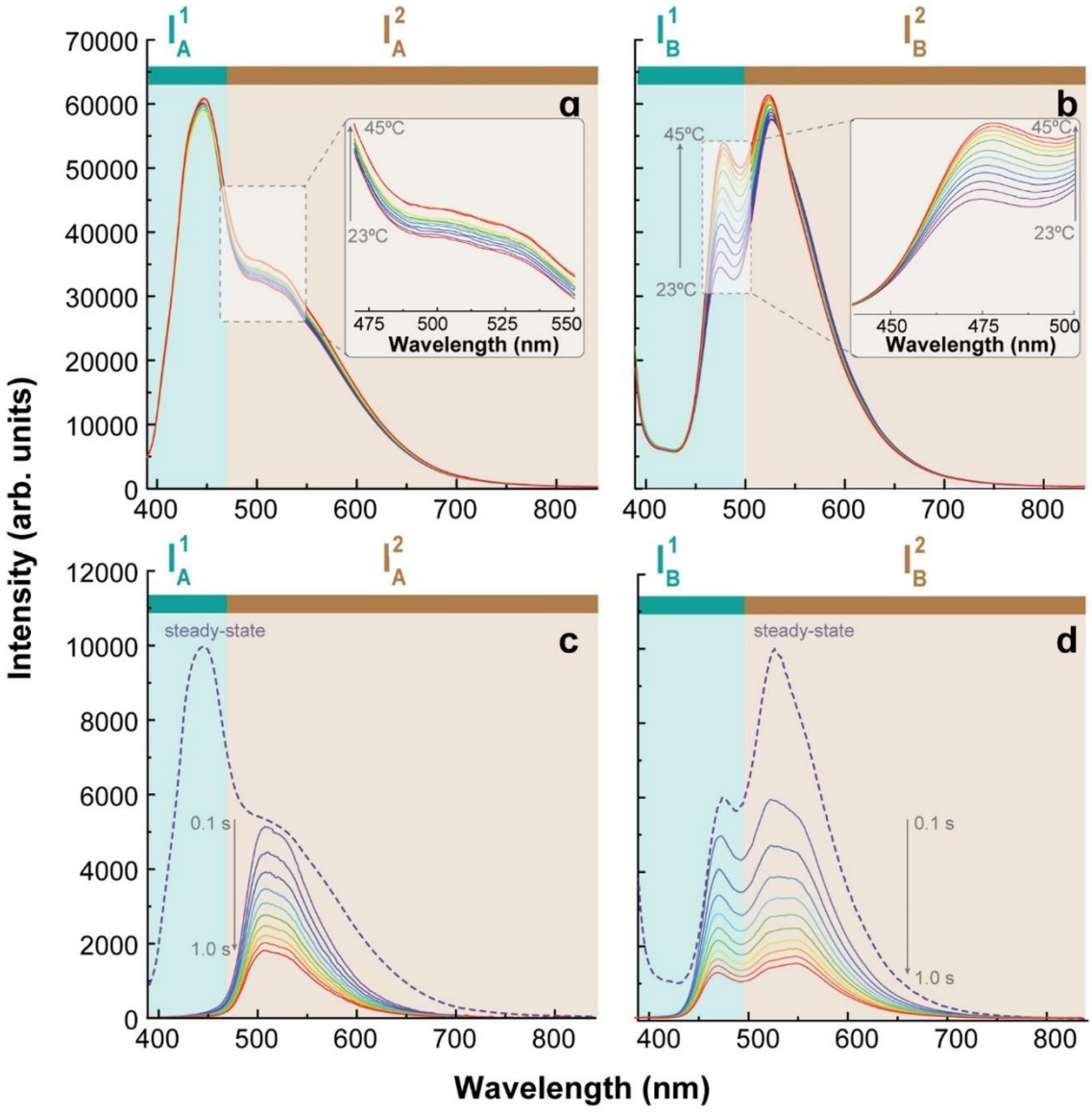

Figure 3.8 Characteristics of the emission with the changing of temperature (λ_{exc} = 365 nm in the steady-state regime) of (a) CD_A and (b) CD_B. Panels (c) and (d) display the temporal behavior at 23 °C of CD_A and CD_B, respectively. The integrated intensity areas I^1 and I^2 define the thermometric parameters for pure e-tags CD_A and CD_B.

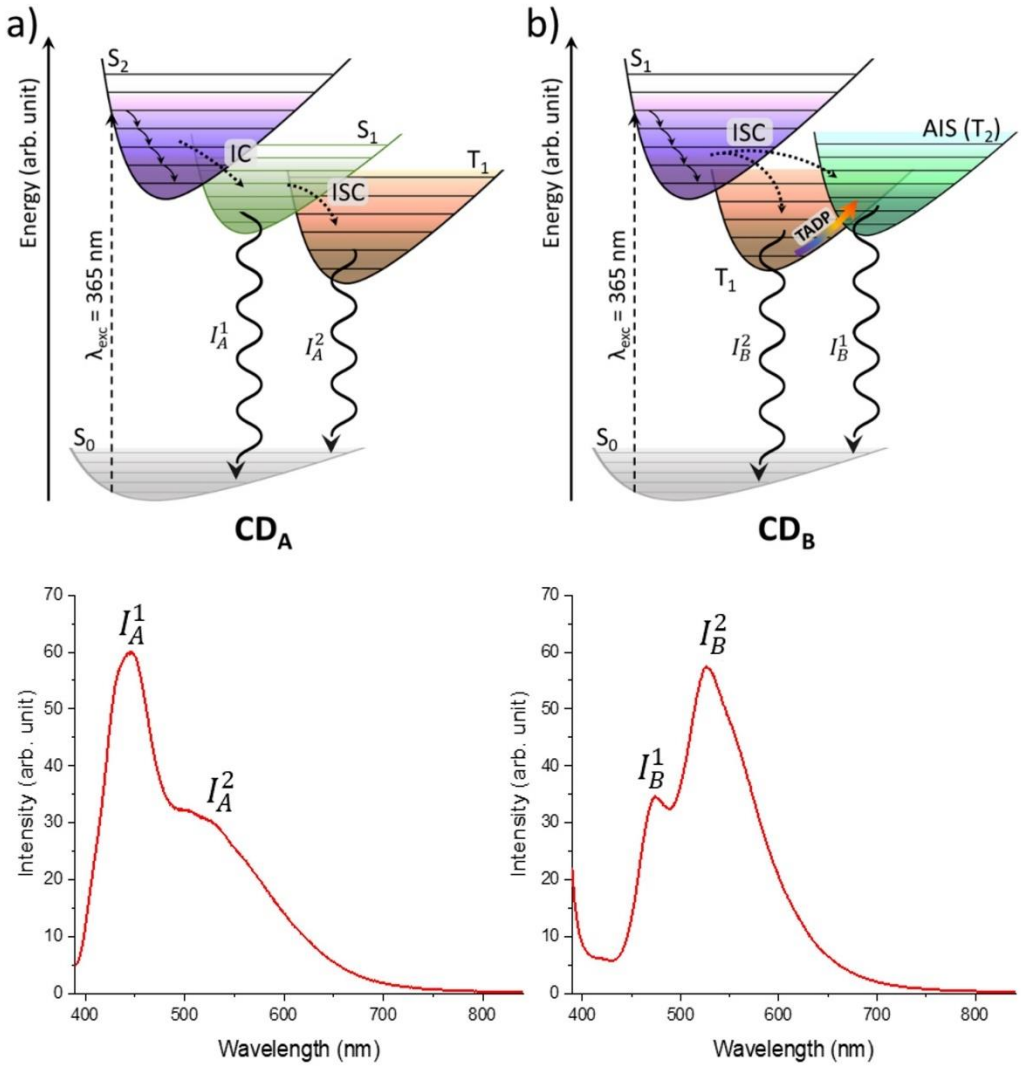

Figure 3.9 a) CD_A exhibits absorption to a second singlet state (S_2), which may decay to the first singlet state (S_1) through an internal conversion (IC) process. Subsequently, S_1 may decay radiatively ($S_1 \rightarrow S_0$ fluorescence, I_A^1) and populate the low-energy triplet state (T_1) via an intersystem crossing (ISC) process. T_1 then decays radiatively ($T_1 \rightarrow S_0$ phosphorescence, I_A^2). b) CD_B displays absorption to the first singlet state (S_1), which can populate both the T_1 level and the AIS. With increasing temperature, T_1 may also populate AIS through a TADP process. The phosphorescence emissions involving these two states are represented as I_B^2 and I_B^1.

The emission spectra of the mixed e-tags reveal the precursors'emission characteristics (**Figure 3.10),** which are affected by their relative intensity dependent on the A:B ratio. For example, in **Figure 3.10**, the high-energy component (389–450 nm, I_{AB}^1) is a clear indication of the fluorescence emission of CD_A, as evidenced by its faster decay, present in all the mixed e-tags (**Figure 3.10-d-f**). Moreover, due to the lower relative amount of CD_A in CD_{14}, it exhibits relatively lower intensity I_{14}^1 (389–450 nm) compared to the I_{41}^1 emission observed in CD_{41} (**Figure 3.10-c**), which lacks the TADP emission characteristic of CD_B. The presence of the TADP process becomes evident when the thermally activated emission band around 475 nm does not increase with temperature, which is particularly noticeable with a lower amount of CD_B, in the mixed CD_{AB} samples (CD_{11} and CD_{41}), as shown in **Figures 3.10-a** and **3.10-c**. Despite the distinct emission

maxima, an interesting observation is that while CD_A exhibits both fluorescence and phosphorescence emissions, CD_B is predominantly characterized by phosphorescent emission (I_{AB}^2 and I_{AB}^3). Even in physical mixtures, energy transfer between CDs and processes like triplet-triplet annihilation or other quenching channels, such as electron-phonon coupling may also occur, implying that the underlying interactions with CDs are complex and multifaceted (*90*, *98*, *103*, *104*).

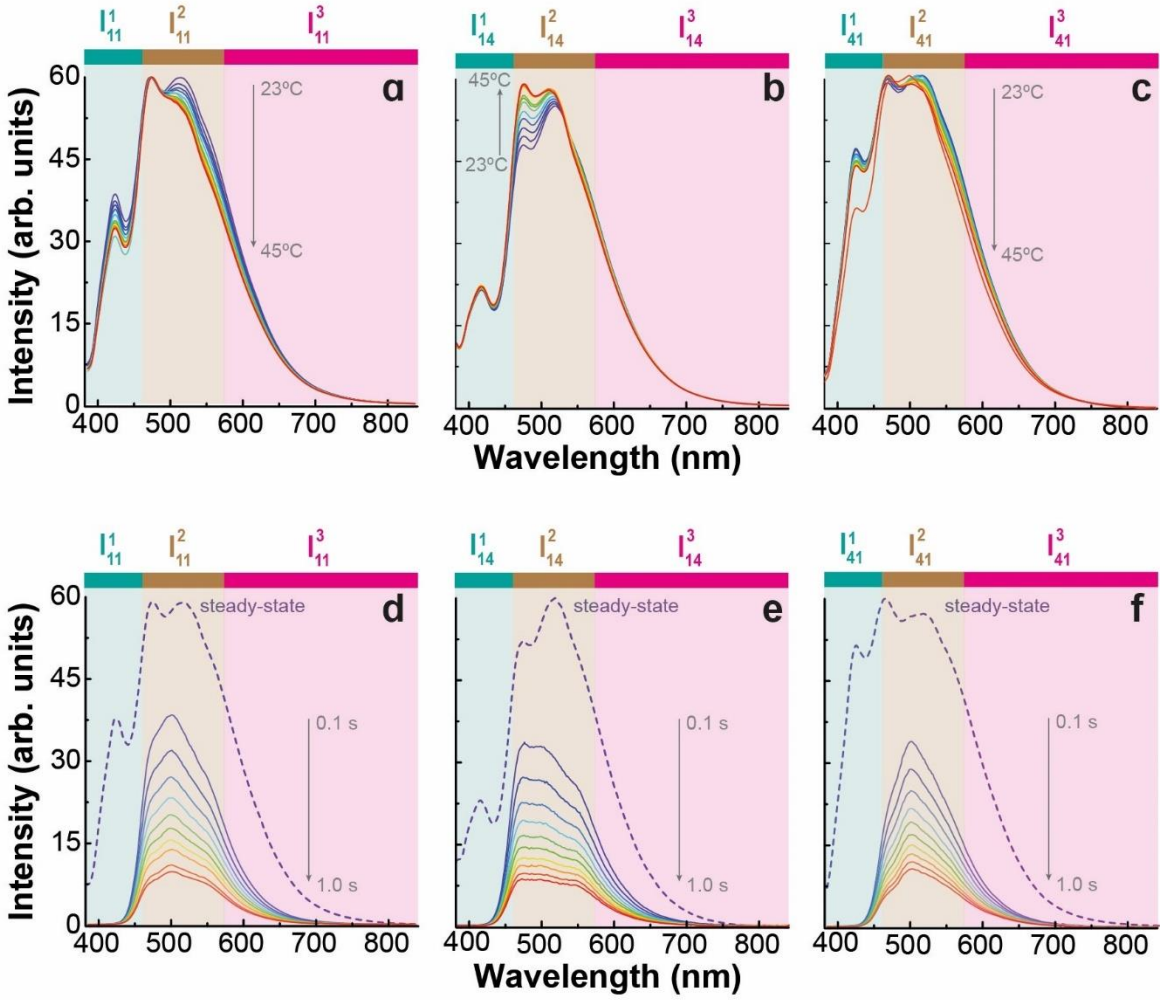

Figure 3.10 Characteristics of the emission with the changing of temperature (excited 365 nm in the steady-state regime) of (a) CD_{11}, (b) CD_{14}, and (c) CD_{41}. Panels (d), (e), and (f) display the respective temporal behavior at 23 °C. The integrated intensity areas I_{AB}^1, I_{AB}^2, and I_{AB}^3 define the thermometric parameters for the mixed CD_{AB}.

Chapter 4. Luminescent e-tags for temperature sensing

This chapter explores the utilization of luminescent e-tags for temperature detection. The chapter is structured into: **Section 4.1** provides a comprehensive explanation of the approach used to capture images and videos using smartphone CCD cameras under various excitation conditions and **Section 4.2** investigates the development of ratiometric thermometric parameters based on emission spectra and luminescent images.

4.1. Image acquisition and processing of the luminescent e-tags

The luminescent e-tags were photographed using a smartphone camera (Zenfone 3, Asus ®) under portable UV excitation (365 nm) or illumination with the smartphone's built-in flash. Under the same conditions, videos were recorded using a smartphone camera (Mi 10T, Xiaomi®) with a resolution of 64 megapixels and was equipped with 6 different types of lenses, all with an aperture of f/1.89. The main camera sensor is a 1/1.7" Sony® IMX682 sensor that utilizes 4-in-1 technology (Super Pixel), which combines four adjacent pixels (0.8 μm each) into a single pixel measuring 1.6 μm. The phosphorescence videos were recorded at 30 frames per second after the excitation was turned off. Each frame (interval 0.03 s) was cropped in 55×45 pixels and analyzed according to the RGB (red, green, blue) color model. A Matlab® routine was used as a tool to perform the RGB analysis.

This model segments images into three channels, each representing a primary color (red, green and blue), enabling the calculation of RGB coordinates. It is best suited for color manipulation and image processing on computer displays. These coordinates allow the quantification of color changes in materials exhibiting temperature-dependent luminescence properties (*50*, *69*). Smartphone cameras, which can effectively capture and analyze color variations (*50*), provide a convenient alternative to specialized equipment such as spectrometers for temperature measurement. Given the widespread use of smartphones equipped with cameras capable of capturing images and videos, they are useful tools for monitoring color changes in luminescent materials, providing information on temperature data fluctuations. Integrating smartphone technology enhances user experience by simplifying temperature quantification processes, rendering them more accessible and adaptable to a variety of applications, including the IoT networks (*69*).

4.2. Thermometric parameters

One of the remarkable features of CDs is their optical response in the UV and visible spectral ranges. This response can be probed using several commercial LEDs or even the flashlights from smartphones. The versatility of these light sources allows for widespread accessibility in different experimental setups. The time-gated detection, revealing emission seconds post-exciting source cessation (t), adds another layer arising from using photoluminescent CDs with phosphorescence emission. The responses are the emission spectra or the luminescent images. Multiple layers of thermal sensing are provided by a single e-tag by exploring various excitation energies and temporal properties that are available with smartphones and portable spectrometers. **Figure 4.1** illustrates the mechanism by which thermometric parameters can be obtained.

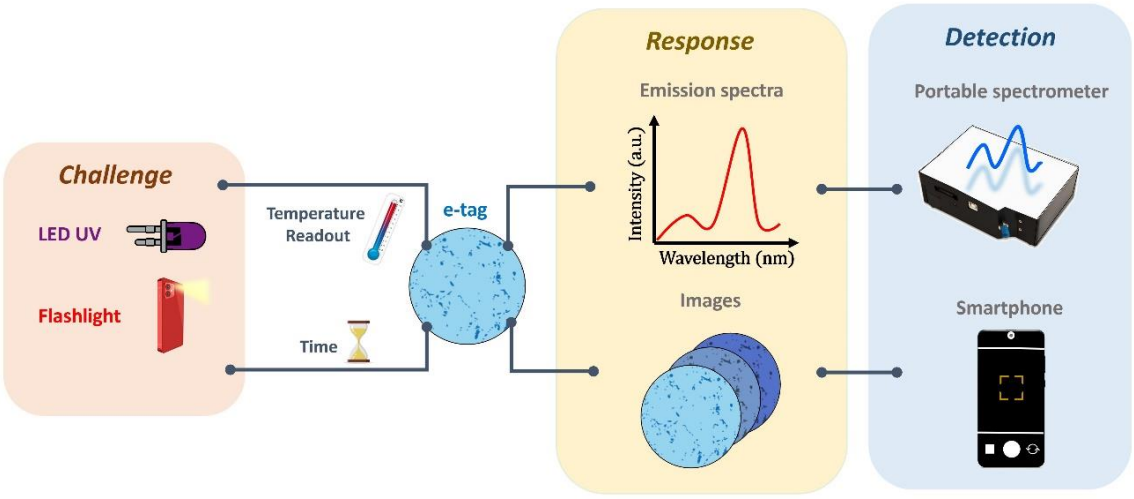

Figure 4.1 Scheme explaining that the thermometric parameters can be achieved either by using a LED UV or by using the flashlight of a smartphone and the responses are based on either the emission spectra or luminescent images acquired when the excitation is turned on and off.

In this dissertation, photonic thermometric parameters were developed using a sample set comprising up to 660 emission spectra and 8,168 photographs captured with a smartphone. The S_r values were determined, and the high values achieved exceed the current state of the art. This supports the potential of our combined approach to advance a new generation of ubiquitous, reliable, and high-performance mobile optical temperature sensors. Taking advantage of the long-lived luminescence decay times and the demonstrated alterations in luminescence properties in response to changes in temperature (T, ºC) and the time delay for optical readings (t, seconds), our objective is to develop nanoscale sensors that establish connections with both T and t as independent variables for optical readings, introducing two-dimensional ratiometric parameters Δ(T,t) (*Equation 4.1* and *Equation 4.2*) to access a 3D response surface of the relative sensitivity parameter, $S_r(T,t)$.

Ratiometric thermometric parameters (Δ) were defined according to the emission spectra' dependence on time and temperature. Thus, distinct ratiometric parameters (*i*=1-36) can be found as a function of the temperature and delay time, $\Delta(T,t)$.

$$\Delta_i(T,t) = \frac{I_{AB}^{\lambda_1}}{I_{AB}^{\lambda_2}} \qquad (4.1)$$

where I_{AB} is the integrated intensity of e-tag CD_{AB} in the low and high-wavelength ranges (λ_1 and λ_2, respectively) of the emission spectra.

The fact that the e-tags from the CD_{AB} samples are excited under the flashlight of the smartphone provides an opportunity to set an additional and complementary number of thermometric parameters ($\Delta_i^{IoT}(T,t)$), *i*=1-30) based on the color change observed in the photographs taken with the smartphone an additional opportunity to build a sensor for mobile sensing including IoT based on the intensity of the RGB color coordinates (I_{RGB} and I'_{RGB}), avoiding the use of expensive and non-ubiquitous equipment (*51*).

$$\Delta_i^{IoT}(T,t) = \frac{I_{RGB}}{I'_{RGB}} \tag{4.2}$$

From equations (4.1) and (4.2) a single e-tag allows the definition of different thermometers providing reliability enhancement through temperature sensing using independent methods. In addition, introducing two-dimensional ratiometric parameters, Δ(T,t) to access a 3D response surface in which the relative sensitivity parameter, $S_r(T,t)$ is defined as:

$$S_r(T,t) = \frac{1}{\Delta(T,t)}\left|\frac{\partial\Delta(T,t)}{\partial T}\right| \tag{4.3}$$

The S_r value represents the variation of the $\Delta(T,t)$ parameter per degree of temperature. Another important parameter is the maximum sensitivity, S_m, which corresponds to the highest value of the S_r, as mentioned before in **Section 2.1.1**. A Python code was developed to conduct a thorough analysis of the input data, involving tasks such as 2D interpolation of points, numerical derivative calculations, and generation of outputs. **Figure 4.2** illustrates the overall procedure used to extract the S_r surface and S_m values for the $\Delta_i(T,t)$. For the $\Delta_i^{IoT}(T,t)$, the procedure was the same, except that in **Figure 4.2-b**, photographs taken with the smartphone were used instead of the emission spectra.

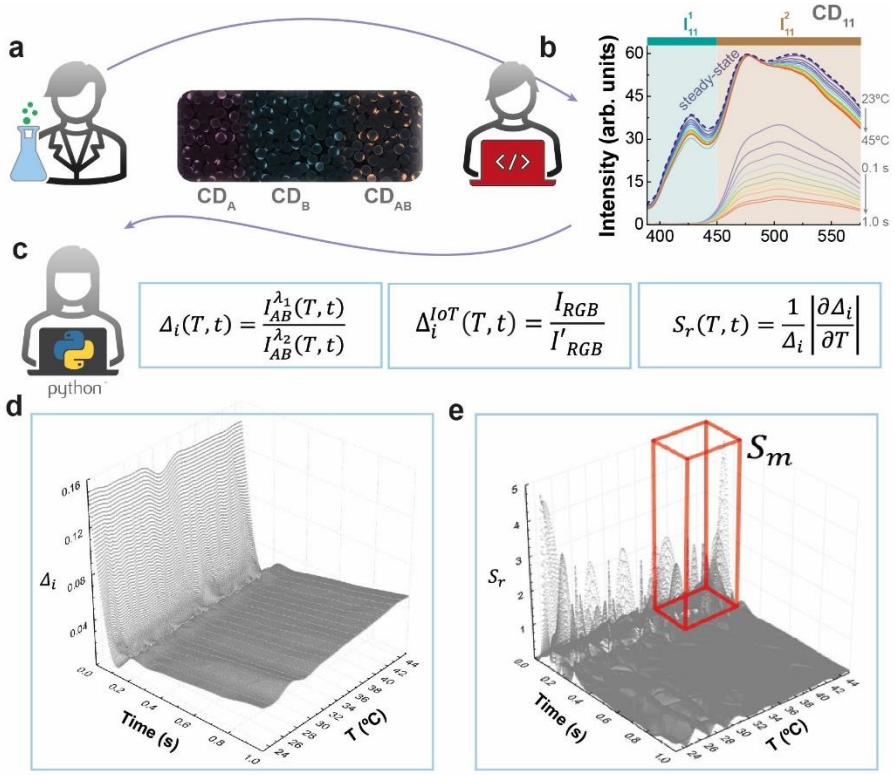

Figure 4.2 (a) Schematics synthesis of pure (CD_A and CD_B) and mixed CD_{AB}; (b) emission spectra as a function of temperature and delay time and shadowed areas related to the (c) definition of $\Delta_i(T,t)$, $\Delta_i^{IoT}(T,t)$ and $S_r(T,t)$. (d) Interpolation of experimental points with a Python code, totaling 2.50×10^4 points per thermometric parameter and (e) relative sensitivity S_r(T,t) obtaining a 3D scatterplot (maximum at S_m).

Table 4.1 provides a comprehensive overview of six distinct definitions of thermometric parameters specifically for pure CDs. Although some may consider them redundant, such as Δ_1 and Δ_2 being reciprocals, their selection is not arbitrary when considering the perspective of relative sensitivity (S_r, *Equation 4.3*). The integrated intensity I_A^1 corresponds to the fluorescence emission for CD_A and I_B^1 to the higher-energy phosphorescence emission of CD_B, which is influenced by the TADP effect (**Figure 3.8**). On the other hand, the integrated intensity I_A^2 represents the phosphorescence bands of CD_A and I_B^2 the lower-energy phosphorescence contribution of CD_B (**Figure 3.8**). This selection enhances the S_r because the derivative of Δ is affected by different emission mechanisms.

Table 4.1 Definitions of the thermometric parameter for CD_A and CD_B. The integrated intensities I_A^1, I_A^2, I_B^1, and I_A^2 are depicted in **Figure 3.8**.

	Thermometric parameter	Definition
CD_A	Δ_1	I_A^1/I_A^2
	Δ_2	I_A^2/I_A^1
	Δ_3	$I_A^1/(I_A^1+I_A^2)$
	Δ_4	$I_A^2/(I_A^1+I_A^2)$
	Δ_5	$(I_A^2+I_A^1)/ I_A^1$
	Δ_6	$(I_A^2+I_A^1)/ I_A^2$
CD_B	Δ_1	I_B^1/I_B^2
	Δ_2	I_B^2/I_B^1
	Δ_3	$I_B^1/(I_B^1+I_B^2)$
	Δ_4	$I_B^2/(I_B^1+I_B^2)$
	Δ_5	$(I_B^2+I_B^1)/ I_B^1$
	Δ_6	$(I_B^2+I_B^1)/ I_B^2$

For mixed CDs, the selection of emissions $I_{A:B}^1$, $I_{A:B}^2$, and $I_{A:B}^3$ (**Figure 3.10**) were specifically made as shown in **Table 4.2** to spectrally overlap with the R, G, B components. Specifically, **Table 4.1** contains the values of Δ_n with n ranging from 1 to 6 for CD_A and CD_B, while **Table 4.2** includes Δ_n with n ranging from 1 to 30 for mixed CD_{AB}.

Table 4.2 Definitions of the thermometric parameters for CD_{11}, CD_{14}, and CD_{41}, as well as definitions for the RGB thermometric parameters acquired through both the phone flash and UV lamp illumination. The integrated intensities I_{AB}^{1} (389 – 450 nm), I_{AB}^{2} (450 – 575 nm), and I_{AB}^{3} (575 – 841 nm) are represented in **Figure 3.10**.

Mixed CDs		Processed e-tags	
Spectroscopic	Integrated intensity	UV (365 nm) or flash	RGB coordinates
Δ_1	I_{AB}^{1}/I_{AB}^{2}	Δ_1^{IoT}	B/G
Δ_2	I_{AB}^{1}/I_{AB}^{3}	Δ_2^{IoT}	B/R_{mean}
Δ_3	I_{AB}^{2}/I_{AB}^{3}	Δ_3^{IoT}	G/R_{mean}
Δ_4	I_{AB}^{2}/I_{AB}^{1}	Δ_4^{IoT}	G/B
Δ_5	I_{AB}^{3}/I_{AB}^{1}	Δ_5^{IoT}	R_{mean}/B
Δ_6	I_{AB}^{3}/I_{AB}^{2}	Δ_6^{IoT}	R_{mean}/G
Δ_7	$I_{AB}^{1}/(I_{AB}^{1}+I_{AB}^{2})$	Δ_7^{IoT}	B/(B+G)
Δ_8	$I_{AB}^{1}/(I_{AB}^{1}+I_{AB}^{3})$	Δ_8^{IoT}	$B/(B+R_{mean})$
Δ_9	$I_{AB}^{1}/(I_{AB}^{2}+I_{AB}^{3})$	Δ_9^{IoT}	$B/(G+R_{mean})$
Δ_{10}	$I_{AB}^{1}/(I_{AB}^{1}+I_{AB}^{2}+I_{AB}^{3})$	Δ_{10}^{IoT}	$B/(B+G+R_{mean})$
Δ_{11}	$I_{AB}^{2}/(I_{AB}^{1}+I_{AB}^{2})$	Δ_{11}^{IoT}	G/(B+G)
Δ_{12}	$I_{AB}^{2}/(I_{AB}^{1}+I_{AB}^{3})$	Δ_{12}^{IoT}	$G/(B+R_{mean})$
Δ_{13}	$I_{AB}^{2}/(I_{AB}^{2}+I_{AB}^{3})$	Δ_{13}^{IoT}	$G/(G+R_{mean})$
Δ_{14}	$I_{AB}^{2}/(I_{AB}^{1}+I_{AB}^{2}+I_{AB}^{3})$	Δ_{14}^{IoT}	$G/(B+G+R_{mean})$
Δ_{15}	$I_{AB}^{3}/(I_{AB}^{1}+I_{AB}^{2})$	Δ_{15}^{IoT}	$R_{mean}/(B+G)$
Δ_{16}	$I_{AB}^{3}/(I_{AB}^{1}+I_{AB}^{3})$	Δ_{16}^{IoT}	$R_{mean}/(B+R_{mean})$
Δ_{17}	$I_{AB}^{3}/(I_{AB}^{2}+I_{AB}^{3})$	Δ_{17}^{IoT}	$R_{mean}/(G+R_{mean})$
Δ_{18}	$I_{AB}^{3}/(I_{AB}^{1}+I_{AB}^{3}+I_{AB}^{2})$	Δ_{18}^{IoT}	$R_{mean}/(B+G+R_{mean})$
Δ_{19}	$(I_{AB}^{1}+I_{AB}^{2})/ I_{AB}^{1}$	Δ_{19}^{IoT}	(B+G)/B
Δ_{20}	$(I_{AB}^{1}+I_{AB}^{3})/ I_{AB}^{1}$	Δ_{20}^{IoT}	$(B+R_{mean})/B$
Δ_{21}	$(I_{AB}^{2}+I_{AB}^{3})/ I_{AB}^{1}$	Δ_{21}^{IoT}	$(G+R_{mean})/B$

Table 4.2 Continued...

Mixed CDs		Processed e-tags	
Spectroscopic	Integrated intensity	UV (365 nm) or flash	RGB coordinates
Δ_{23}	$(I^1_{AB}+I^2_{AB})/ I^2_{AB}$	Δ^{IoT}_{23}	(B+G)/G
Δ_{24}	$(I^1_{AB}+I^3_{AB})/ I^2_{AB}$	Δ^{IoT}_{24}	$(B+R_{mean})/G$
Δ_{25}	$(I^2_{AB}+I^3_{AB})/ I^2_{AB}$	Δ^{IoT}_{25}	$(G+R_{mean})/G$
Δ_{26}	$(I^1_{AB}+I^3_{AB}+I^2_{AB})/ I^2_{AB}$	Δ^{IoT}_{26}	$(B+G+R_{mean})/G$
Δ_{27}	$(I^1_{AB}+I^2_{AB})/ I^3_{AB}$	Δ^{IoT}_{27}	$(B+G)/ R_{mean}$
Δ_{28}	$(I^1_{AB}+I^3_{AB})/ I^3_{AB}$	Δ^{IoT}_{28}	$(B+R_{mean})/ R_{mean}$
Δ_{29}	$(I^2_{AB}+I^3_{AB})/ I^3_{AB}$	Δ^{IoT}_{29}	$(G+R_{mean})/ R_{mean}$
Δ_{30}	$(I^1_{AB}+I^3_{AB}+I^2_{AB})/ I^3_{AB}$	Δ^{IoT}_{30}	$(B+G+R_{mean})/ R_{mean}$

Figure 4.3 summarizes the overall values of S_m for all ratiometric parameters based on the emission features measured with the spectrometer. It is evident that pure CDs exhibit lower values of S_m, with a maximum for CD_A with Δ_5 (S_m = 1.63 %·°C^{-1}, **Table 4.3** and inset **Figure 4.3-b**), compared to the mixed one CD_{41} which displays S_m = 7.89 %·°C^{-1} (**Table 4.3** and **Figure 4.3-b**). Furthermore, CD_A and CD_B have a disadvantage of having their values of S_m values occur at very restricted delay times (0.0 – 0.1 s) and lower temperatures (23 – 25 °C), as shown in inset **Figure 4.3-a**. The physical mixed e-tags (CD_{41}, CD_{11}, and CD_{14}) reveal superior performance concerning the S_m values compared to the precursors over a wide temperature operating range (**Figure 4.3-b**).

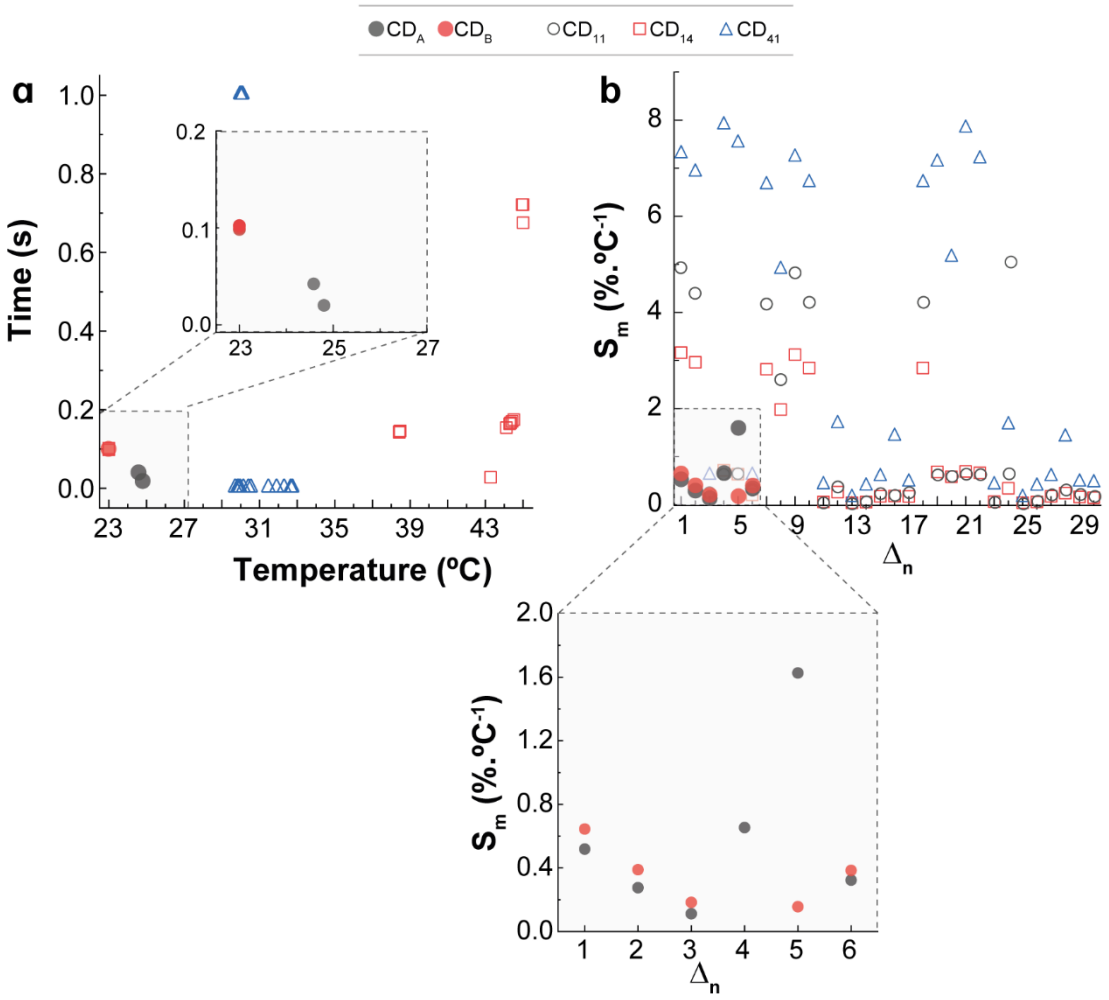

Figure 4.3 (a) Distribution of S_m based on delay time and temperature. (b) Maximum relative sensitivity (S_m) values for CD_A and CD_B, and for the mixed e-tags CD_{11}, CD_{14}, and CD_{41}

Table 4.3 compares the S_m values obtained from CD-based thermometers using spectroscopic techniques as reported in the literature to those obtained in this dissertation. The results demonstrate significantly higher values for the physical mixtures of CD_A and CD_B than previous reports. For instance, a core-shell $Gd(OH)CO_3$-cys-CD@$mSiO_2$-RhB nanocomposite system presents the highest reported S_r value of 1.39 %·°C^{-1} (*105*). However, the purposed multiparametric approach and the emission time result in higher S_r values for all mixed CDs and CD_A (**Table 4.3**) ranging from 1.63 %·°C^{-1} for CD_A (Δ_5, **Table 4.1**) to 7.89 %·°C^{-1} for CD_{41} (using $\Delta_4 = I_{14}^2/I_{14}^1$, **Table 4.2**).

Table 4.3 Comparison of S_m values found in the literature for CD-based thermometers. Maximum value of the S_r (i.e., S_m) and the temperature at which it occurs. All data were collected using spectroscopic techniques (**cys**=L-cystine, **RhB=B**=Rhodamine B, **ZAO**=$ZnAl_2O_4$, **CLNO**=Ca_2LaNbO_6, **ZIF=**zeolitic-imidazolate-framework, **dU6=**di-ureasil, **MMM**=mixed-matrix membrane, **BiOCl**=bismuth oxychloride).

Designation	S_m (%·°C^{-1})	T (°C)
CD_A this dissertation	1.63	23
CD_B this dissertation	0.64	23
CD_{11} this dissertation	4.96	23
CD_{14} this dissertation	3.16	23
CD_{41} this dissertation	7.89	33
Gd(OH)CO_3-cys-CD@mSiO_2-RhB (*105*)	1.39	100
CDs@ZAO:Eu (*106*)	0.11	110
CLNO:0.5%Pr (*107*)	0.79	175
CLNO:3%Pr (*107*)	0.89	250
CLNO:9%Pr (*107*)	0.69	175
CDs&RB@ZIF-8[2]-MMM (*108*)	0.74	20
dU6/CD-RhD (*93*)	1.03	45
CDs/BiOCl (*109*)	1.35	20

Despite having consistently higher S_m values on average, CD_{41}'s maximum sensitivity is restricted to the range 30-33 °C (**Figure 4.3-d**), considering all thermometric parameters (Δ_i with i=1-30, **Table 4.2**). Among all the mixed CDs, CD_{14} contains a higher proportion of RhB-based CDs (CD_B). Surprisingly, the presence of TADP has a negative impact on the thermometric response, as evidenced by the trend of higher amounts of CD_B correlated with lower thermometric performance. Moreover, there is a synergistic interaction between CD_A and CD_B, which results in improved performance in mixed CDs, as demonstrated by an increase in thermometric performance from pure CD_A to the mixed CD_{AB} samples, even for the case of CD_{14}. The CD_{11} has the best performance and emerges as a promising candidate for application in mobile sensing. Consequently, CD_{11} was selected for preparing the e-tags and conducting mobile sensing experiments using a smartphone and portable excitation sources.

The photographs in **Figure 4.5-a** illustrate the afterglow exhibited by the e-tags over time when the excitation sources are turned off, showcasing their emission after the excitation was tuned off, which is still detectable using a smartphone camera. This intrinsic property underscores the potential applications of these materials in environments with low-light conditions or for energy-saving purposes. Additionally, **Figure 4.5-b** displays the temperature-dependent luminescence behavior (t=0.6 s fixed), in which the RGB intensity is thermally dependent. Employing mobile detection, we quantified the emission color by analyzing the RGB color coordinates and computing the thermometric performance, **Figure 4.5-c-f**.

The dominant intensity was observed for the B and G coordinates, while the R coordinate values were significantly lower. The mobile thermometric parameter $\Delta_i^{IoT}(T,t)$ was calculated by

measuring the RGB intensity as a function of the temperature and time, as illustrated in Figure **4.4 a-d** and **Figure 4.5-c-f**. Using UV lamp as the excitation source, it was achieved an outstanding S_m value of 7.81 %·°C^{-1} at T = 29 °C and t = 4.81 s (**Figure 4.4-b**) for the thermometric parameter Δ_5^{IoT}(**Figure 4.4-a**) Similarly, using the smartphone flashlight as the excitation source, the thermometric parameter Δ_3^{IoT} (**Figure 4.4-c**) presents a S_m value of 3.51 %·°C^{-1} at T = 45 °C and t = 2.89 s (**Figure 4.4 d**). Despite having the highest S_m values among the 60 thermometric parameters calculated, Δ_5^{IoT}(UV lamp as excitation source) and Δ_3^{IoT} (Flash lamp as excitation source) were determined using the R coordinate.

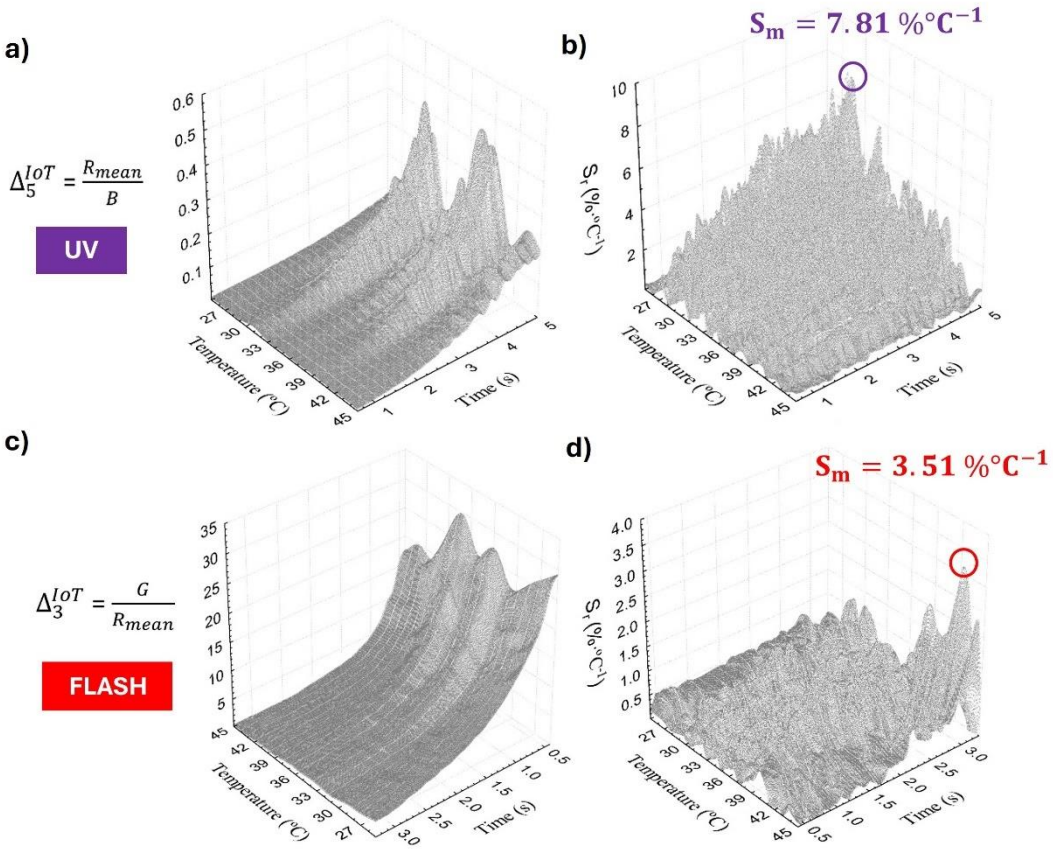

Figure 4.4 Thermometric scatterplots of a) $\Delta_5^{IoT} = \mathrm{R_{mean}/B}$ under UV lamp excitation and (c) $\Delta_3^{IoT} = \mathrm{G/R_{mean}}$ under phone flash excitation. Their associated S_r values are shown in panels (b) and (d), respectively. The values of S_m are highlighted.

Thus, to investigate the correlation between the intensity of B and G coordinates, the $\Delta_4^{IoT} = G/B$ case is depicted in the **Figure 4.5-c-f.** The values of S_m, shown in **Figure 4.5-d,f**, remain higher than those found in the literature using traditional and expensive spectroscopic equipment (**Table 4.3**). This finding emphasizes the practical applicability of these e-tags, indicating a promising future in the application of CDs in luminescent thermometers based on the methodology presented in this dissertation.

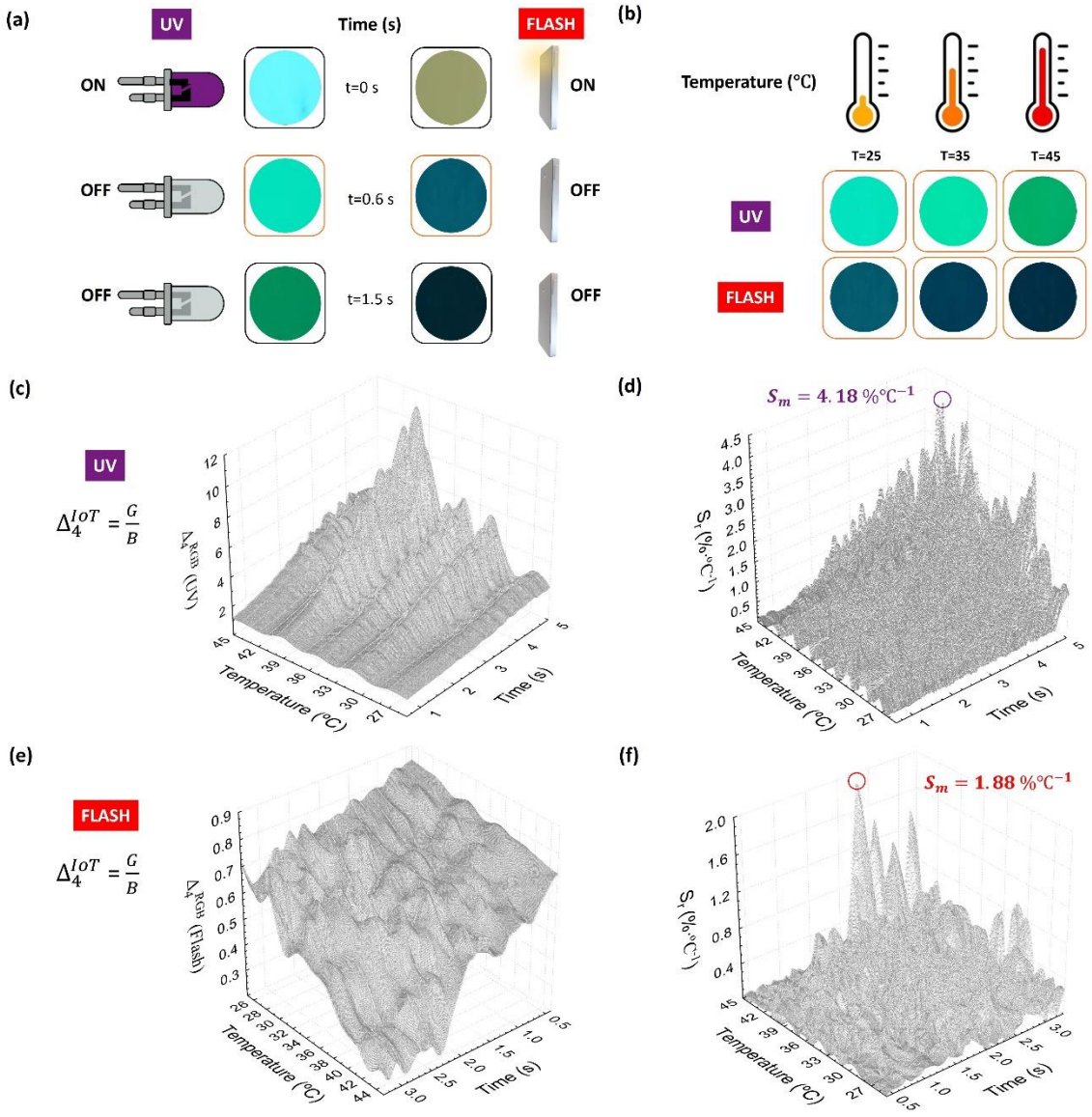

Figure 4.5 (a) Sequential photographs capturing the progression of the CD_{11}-based e-tag over time at 25 °C. At the starting point (t = 0 s), the sample was stimulated by the UV lamp (on the left) and the mobile phone flash (on the right). Subsequently, the illumination sources were promptly deactivated, and the subsequent photographs were recorded at t = 0.6 and 1.5 seconds. (b) Photographs of the e-tag showing variations at different temperatures (25, 35, and 45 °C) with a fixed time t = 0.6 s. Thermometric scatterplots of $\Delta_4^{IoT} = G/B$ under (c) UV lamp and (e) phone flash excitations. Their associated S_r values are shown in panels (d) and (f), respectively. The values of S_m are highlighted.

Chapter 5. Conclusions and Future Work

Innovative temperature sensors are crucial in biomedical engineering, especially for e-health. As our understanding of the body grows, the need for precise, real-time physiological data becomes clear. Temperature, a key health indicator, aids in diagnosing, treating, and preventing many conditions. From detecting fevers to monitoring critical patients, temperature is vital for care planning. As a biomedical engineer, my goal is to create solutions that advance digital health. With technology transforming our lives, the potential to revolutionize monitoring with new materials and sensing technologies is vast. This dissertation explores novel luminescence thermometry approaches using different mixtures of CDs to improve on conventional methods. Luminescence thermometry, using the unique properties of luminescent materials, offers a transformative, non-invasive approach to temperature measurement, ideal for portable devices like smartphones. This technology could revolutionize mobile health monitoring, enabling patients to easily track temperatures at home and providers to access real-time data remotely. However, robust protocols are needed to ensure accuracy despite environmental factors. This research aims to enhance the reliability of luminescent thermometers for real-time use, paving the way for seamless smartphone integration and continuous, user-friendly monitoring.

This dissertation underscores the multifaceted utility of carbon CDs in luminescent thermometry, showcasing their exceptional properties such as robust luminescence, resistance to photobleaching, and chemical stability. The versatility and tunability of CDs make them an ideal platform for thermometric applications. By synthesizing CDs from dibenzoylmethane (CD_A) and Rhodamine B (CD_B) precursors, their potential as thermometric materials were demonstrated in **Section 3.1.1**, particularly in mixed configurations. CD_A and CD_B, each exhibiting distinct emissive properties, alongside physical mixtures with varying A:B ratios, offer a rich spectrum suitable for thermometric measurements. The synergistic interaction between CD_A and CD_B was highlighted, resulting in improved thermometric performance in mixed CDs, which show emission characteristics dependent on the ratio of CD_A to CD_B. The high-energy component is dominated by CD_A fluorescence emission, while CD_B contributes mainly with phosphorescent emission. However, this intriguing synergistic interaction between CD_A and CD_B warrants further investigation, particularly focusing on energy transfer calculations involving CDs in diluted systems (*98*). Elucidating the fundamental photophysics underlying this synergy will be crucial to fully harness the potential of mixed CD systems. By delving deeper into the synergetic interactions that enhance thermometric performance, we can develop a more comprehensive understanding of how to optimize these materials for various temperature ranges and conditions. This could be a topic to explore in future work.

Additionally, by studying their luminescent characteristics, it is shown not only that the emission spectra of the CDs and mixed e-tags vary with temperature, indicating potential for thermal sensing applications and but also the e-tags exhibit phosphorescence emission behavior characterized by long lifetimes (**Section 3.3.3**), allowing for the incorporation of emission acquisition time as an additional parameter in thermometric analysis, leading to the development of a novel ratiometric parameter, Δ(T,t), deviating from traditional ratiometric thermometers and to the generation of a 3D response surface of the relative sensitivity parameter, S_r(T,t) (**Subchapter 4.2**). This dissertation elucidates the influence of AIS and TADP effect, which are particularly prominent in CD_B and mixtures with a high Rhodamine B content (CD_{14}). By fine-tuning the proportion of CD_A and CD_B in mixed CDs, the TADP effect can be adjusted to optimize thermometric parameters (**Section 3.3.3**). The thermometry performance analysis of over 100 defined ratiometric parameters further

underscores the potential of these materials, with parameters exhibiting high relative sensitivities (up to 7.9 %·°C^{-1}) in the critical temperature range of 23 – 45 °C. These findings demonstrate the remarkable promise of CDs as thermometric materials, rivaling the performance of more established luminescent species. Future work could also focus on enhancing the photostability and sensitivity of CDs to ensure reliable long-term usage in diverse environments.

Finally, the practical applications of luminescent CDs were investigated by exploring their thermometric performance in the RGB model and fabricating e-tags based on CD_{11} (**Subchapter 4.1**). The analysis RGB allows for quantifying color changes in materials with temperature-dependent luminescence properties. The CDs exhibit strong absorption in the UV and visible regions, making them suitable for excitation with low-power light sources (**Section 3.3.1**). This is a critical consideration for real-world applications, where robust performance under varied ambient conditions is paramount. The thermometric performance of pure CDs (CD_A and CD_B) and mixed CDs (CD_{11}, CD_{14}, CD_{41}) was evaluated and the responses are based on either the emission spectra or luminescent images acquired when the excitation is turned on and off. The e-tags exhibited afterglow and temperature-dependent luminescence behaviors, detectable with smartphone cameras even in low-light conditions. Using a UV lamp as the excitation source, this e-tag achieved an exceptional sensitivity value of $S_m = 7.81$ %·°C^{-1} at T = 29 °C and t = 4.81 s. Similarly, employing the phone flash as the excitation source yielded a value of $S_m = 3.51$ %·°C^{-1} at T = 45 °C and t = 2.89 s. By focusing on the dominant emission in the B and G coordinates, it was also observed improved thermal performance, reaching 4.18 and 1.88 %·°C^{-1} for the UV lamp and phone flash, respectively (**Subchapter 4.2**). These values surpass those reported in the literature for CD-based thermometers utilizing traditional spectroscopic equipment, despite the inherent limitations of smartphone camera detection.

This dissertation demonstrates the potential of luminescent e-tags for cost-effective temperature sensing using smartphone LEDs. The e-tags' prolonged phosphorescence highlights their suitability for low-light or energy-efficient applications. As the Internet of Things (IoT) and wearables advance, e-tags could enable next-generation health monitors. This research provides valuable insights into developing temperature sensing technologies with luminescent materials for e-health and m-health applications. The findings could lead to innovative, real-time temperature monitoring devices benefiting medical professionals. The CD-based e-tags in this dissertation were processed as pellets, but they are versatile enough to be printed (using methods such as inkjet printing, spraying, spin-coating, and drop casting) on a variety of substrates including paper, plastic, and textiles, like printable electronic circuits. Future work could focus on designing optimal smart e-tags for the luminescent thermometers discussed in this study, enhancing their practicality and expanding their application range. The technology's potential to transform healthcare is vast, from early disease detection in resource-poor areas to empowering patient self-monitoring.

In conclusion, this dissertation primary goal has been successfully achieved with the creation of robust luminescent thermometers for real-time, smartphone-integrated e-health applications. This paves the way for continuous, user-friendly temperature monitoring, advancing mobile and personalized healthcare. The findings underscore the immense promise of this technology for making health monitoring more accessible, accurate, and patient-centered through biomedical engineering innovations towards e-Health.

References

1. L. Xie *et al.*, *Preventive Medicine*. **157**, 13 (2022).
2. N. Kalid *et al.*, *Journal of Medical Systems*. **42**, 30 (2018).
3. G. Aceto, V. Persico, A. Pescapé, *Journal of Network and Computer Applications*. **107**, 125–154 (2018).
4. L. P. Malasinghe, N. Ramzan, K. Dahal, *Journal of Ambient Intelligence and Humanized Computing*. **10**, 57–76 (2019).
5. J. F. C. B. Ramalho, A. N. C. Neto, L. D. Carlos, P. S. André, R. A. S. Ferreira, *Handbook on the Physics and Chemistry of Rare Earths (Including Actinides)* (2022), vol. 61.
6. S. Chen *et al.*, *IEEE Internet of Things Magazine*, 12–16 (2021).
7. L. M. S. Dias *et al.*, *IEEE Access*. **10**, 24433–24443 (2022).
8. C. D. S. Brites, S. Balabhadra, L. D. Carlos, *Advanced Optical Materials*. **7**, 1–30 (2018).
9. X. D. Wang, O. S. Wolfbeis, R. J. Meier, *Chemical Society Reviews*. **42**, 7834–7869 (2013).
10. K. M. McCabe, M. Hernandez, *Pediatric Research*. **67**, 469–475 (2010).
11. G. Sullivan, M. Spencer, *BJA Education*. **22**, 350–356 (2022).
12. R. Piñol *et al.*, *Nano Letters*. **20**, 6466–6472 (2020).
13. M. Auinger, D. Vogel, A. Vogel, M. Spiegel, M. Rohwerder, *Review of Scientific Instruments*. **84**, 1–5 (2013).
14. D. Ross-Pinnock, P. G. Maropoulos, *Proceedings of the Institution of Mechanical Engineers, Part B: Journal of Engineering Manufacture*. **230**, 793–806 (2016).
15. R. Judge, F. Choi, B. Helmuth, *Frontiers in Ecology and Evolution*. **6**, 1–18 (2018).
16. K. Okabe, S. Uchiyama, *Communications Biology*. **4**, 1–7 (2021).
17. W. Chen, *Biomedical Engineering Letters*. **9**, 3–17 (2019).
18. J. E. Hall, A. C. Guyton, *Guyton and Hall-Textbook of Medical Physiology* (12th ed., 2011).
19. Y. Khan, A. E. Ostfeld, C. M. Lochner, A. Pierre, A. C. Arias, *Advanced Materials*. **28**, 4373–4395 (2016).
20. J. Kuht, A. D. Farmery, *Anaesthesia and Intensive Care Medicine*. **19**, 507–512 (2018).
21. C. L. Tan, Z. A. Knight, *Neuron*. **98**, 31–48 (2018).
22. Y. Zhao, J. H. M. Bergmann, *Sensors*. **23** (2023).
23. E. Carrasco *et al.*, *Advanced Functional Materials*. **25**, 615–626 (2015).
24. C. Childs, in *Handbook of Clinical Neurology* (2018), vol. 157, pp. 467–482.
25. K. Nakamura, *American Journal of Physiology - Regulatory Integrative and Comparative Physiology*. **301** (2011).
26. Y. Su *et al.*, *Nanoscale Research Letters*. **15** (2020).
27. C. D. S. Brites *et al.*, *New Journal of Chemistry*. **35**, 1177–1183 (2011).
28. A. J. Mah *et al.*, *Biology*. **10**, 1–15 (2021).
29. G. P. Szakmany, A. O. Orlov, G. H. Bernstein, W. Porod, *IEEE Transactions on Nanotechnology*. **13**, 1234–1239 (2014).
30. N. Kong, Q. Hu, Y. Wu, X. Zhu, *Chemistry - A European Journal*. **28** (2022).
31. L. H. J. Raijmakers, D. L. Danilov, F. J. Iek-, D.- Jülich, *Applied Energy*. **240**, 918–945 (2019).
32. J. F. C. B. Ramalho, L. D. Carlos, P. S. André, R. A. S. Ferreira, *Advanced Photonics Research*. **2** (2021).
33. B. B. Lahiri, S. Bagavathiappan, T. Jayakumar, J. Philip, *Infrared Physics and Technology*. **55**, 221–235 (2012).
34. C. D. S. Brites, A. Millán, L. D. Carlos, *Handbook on the Physics and Chemistry of Rare Earths*. **49**, 339–427 (2016).
35. C. D. S. Brites, S. Balabhadra, L. D. Carlos, *Advanced Optical Materials*. **7** (2019).
36. C. Bradac, S. F. Lim, H. Chang, I. Aharonovich, *Advanced Optical Materials*, 1–29 (2020).
37. A. Bednarkiewicz, L. Marciniak, L. D. Carlos, D. Jaque, *Nanoscale*. **12**, 14405–14421 (2020).
38. R. A. S. Ferreira *et al.*, *Laser and Photonics Reviews*. **7**, 1027–1035 (2013).

39. T. P. van Swieten *et al.*, *ACS Applied Nano Materials*. **4**, 4208–4215 (2021).
40. R. G. Geitenbeek *et al.*, *Lab on a Chip*. **19**, 1236–1246 (2019).
41. T. S. Jacobs *et al.*, *ACS Nano*. **17**, 20053–20061 (2023).
42. D. Jaque *et al.*, *Nanomedicine*. **9**, 1047–1062 (2014).
43. A. Nexha, J. J. Carvajal, M. C. Pujol, F. Díaz, M. Aguiló, *Nanoscale*. **13**, 7913–7987 (2021).
44. C. D. S. Brites *et al.*, *Advanced Materials*. **35** (2023).
45. M. Suta *et al.*, *Nanomaterials*. **10**, 543 (2020).
46. C. D. S. Brites, E. D. Martínez, R. R. Urbano, C. Rettori, L. D. Carlos, *Frontiers in Chemistry*. **7**, 1–10 (2019).
47. A. S. Souza *et al.*, *Nanoscale*. **8**, 5327–5333 (2016).
48. A. De *et al.*, *Journal of Materials Chemistry C*. **11**, 6095–6106 (2023).
49. K. M. N. de Souza *et al.*, *Advanced Optical Materials*. **10** (2022).
50. J. F. C. B. Ramalho *et al.*, *Advanced Science*. **6** (2019).
51. J. F. C. B. Ramalho *et al.*, *Advanced Photonics Research*. **3**, 1–11 (2022).
52. A. N. Carneiro Neto *et al.*, *Advanced Optical Materials*. **10** (2022).
53. B. del Rosal *et al.*, *Advanced Functional Materials*. **26**, 6060–6068 (2016).
54. W. U. Khan *et al.*, *ACS Applied Bio Materials*. **4**, 5786–5796 (2021).
55. L. J. Mohammed, K. M. Omer, *Nanoscale Research Letters*. **15**, 1–21 (2020).
56. J. Liu *et al.*, *RSC Advances*. **6**, 47427–47433 (2016).
57. O. A. Savchuk, O. F. Silvestre, R. M. R. Adão, J. B. Nieder, *Scientific Reports*. **9**, 1–11 (2019).
58. C. D. S. Brites *et al.*, *Nanoscale*. **4**, 4799–4829 (2012).
59. D. Zhao *et al.*, *Inorganic Chemistry*. **54**, 11193–11199 (2015).
60. C. Li, Y. Wang, H. Jiang, X. Wang, *Journal of The Electrochemical Society*. **167**, 037540 (2020).
61. W. U. Khan *et al.*, *ACS Applied Bio Materials*. **4**, 5786–5796 (2021).
62. P. Yu, X. Wen, Y. R. Toh, J. Tang, *Journal of Physical Chemistry C*. **116**, 25552–25557 (2012).
63. L. Đorđević, F. Arcudi, M. Cacioppo, M. Prato, *Nature Nanotechnology*. **17**, 112–130 (2022).
64. S. Das, L. Ngashangva, P. Goswami, *Micromachines*. **12**, 1–36 (2021).
65. V. Lojpur, G. Nikolić, M. D. Dramićanin, *Journal of Applied Physics*. **115**, 1–7 (2014).
66. A. Al-Fuqaha, M. Guizani, M. Mohammadi, M. Aledhari, M. Ayyash, *IEEE Communications Surveys and Tutorials*. **17**, 2347–2376 (2015).
67. J. F. C. B. Ramalho *et al.*, *npj Flexible Electronics*. **4** (2020).
68. T. M. Fernandez-Carames, P. Fraga-Lamas, *IEEE Access*. **6**, 25939–25957 (2018).
69. J. F. C. B. Ramalho, L. D. Carlos, P. S. André, R. A. S. Ferreira, *Advanced Photonics Research*. **2** (2021).
70. Y. Zhao, X. Wang, Y. Zhang, Y. Li, X. Yao, *Journal of Alloys and Compounds*. **817** (2020).
71. M. Suta, A. Meijerink, *Advanced Theory and Simulations*. **3**, 1–32 (2020).
72. J. R. Lakowicz, *Principles of fluorescence spectroscopy* (2006).
73. W. K. Szapoczka, A. L. Truskewycz, T. Skodvin, B. Holst, P. J. Thomas, *Scientific Reports*. **13**, 1–11 (2023).
74. K. V. R. Murthy, H. S. Virk, *Defect and Diffusion Forum*. **347**, 1–34 (2014).
75. M. D. Dramićanin, *Journal of Applied Physics*. **128**, 1–19 (2020).
76. E. J. McLaurin, L. R. Bradshaw, D. R. Gamelin, *Chemistry of Materials*. **25**, 1283–1292 (2013).
77. C. D. S. Brites *et al.*, *Advanced Materials*. **22**, 4499–4504 (2010).
78. J. Rocha, C. D. S. Brites, L. D. Carlos, *Chemistry - A European Journal*. **22**, 14782–14795 (2016).
79. F. E. Maturi *et al.*, *Laser and Photonics Reviews*. **15**, 1–10 (2021).
80. S. Choi, V. N. Agafonov, V. A. Davydov, T. Plakhotnik, *ACS Photonics*. **6**, 1387–1392 (2019).
81. Y. Chen *et al.*, *Advanced Photonics Research*. **4** (2023), doi:10.1002/adpr.202300106.
82. I. E. Kolesnikov *et al.*, *Journal of Materials Chemistry C*. **11**, 14814–14825 (2023).

83. J. Zhu, N. Zhao, S. Liu, S. Wei, R. Zhou, *Advanced Photonics Research*. **3**, 9–17 (2022).
84. N. Katumo, G. Gao, F. Laufer, B. S. Richards, I. A. Howard, *Advanced Optical Materials*. **8** (2020).
85. T. Pan, W. Cao, M. Wang, *Optical Fiber Technology*. **45**, 359–362 (2018).
86. Z. Zhu, *Analytica Chimica Acta*. **1054**, 122–127 (2019).
87. P. E. Araque *et al.*, *IEEE Sensors Journal*. **18**, 4351–4357 (2018).
88. D. Zhang, Q. Liu, *Biosensors and Bioelectronics*. **75**, 273–284 (2016).
89. S. Kanchi, M. I. Sabela, P. S. Mdluli, Inamuddin, K. Bisetty, *Biosensors and Bioelectronics*. **102**, 136–149 (2018).
90. L. M. S. Dias *et al.*, *FlexMat*. **1** (2024).
91. Z. Xu *et al.*, *Journal of Materials Chemistry C*. **8**, 4557–4563 (2020).
92. W. He, X. Sun, X. Cao, *ACS Sustainable Chemistry and Engineering*. **9**, 4477–4486 (2021).
93. S. F. H. Correia *et al.*, *Nanoscale Advances*. **5**, 3428–3438 (2023).
94. L. Wang *et al.*, *Nature Communications*. **5**, 1–9 (2014).
95. F. Yuan *et al.*, *Nature Communications*. **9**, 1–11 (2018).
96. Y. Ding, X. Wang, M. Tang, H. Qiu, *Advanced Science*. **9**, 1–9 (2022).
97. X. Xu *et al.*, *Advanced Materials*. **33** (2021).
98. B. S. D. Onishi *et al.*, *Nanoscale*. **16**, 6286–6295 (2024).
99. U. Rocha *et al.*, *Spectrochimica Acta - Part A: Molecular and Biomolecular Spectroscopy*. **317** (2024).
100. C. H. Mak *et al.*, *Advanced Optical Materials*. **8**, 1–9 (2020).
101. Q. Lou *et al.*, *Advanced Materials*. **35**, 1–12 (2023).
102. P. K. Samanta, D. Kim, V. Coropceanu, J.-L. Brédas, *Journal of the American Chemical Society*. **139**, 4042–4051 (2017).
103. L. Naimovičius, P. Bharmoria, K. Moth-Poulsen, *Materials Chemistry Frontiers*. **7**, 2297–2315 (2023).
104. J. Tan *et al.*, *Nanoscale*. **8**, 4742–4747 (2016).
105. Z. Zhu, Z. Sun, Z. Guo, X. Zhang, Z. Wu, *Journal of Colloid and Interface Science*. **552**, 572–582 (2019).
106. S. H. Yang, S. M. Liao, Y. Y. Tsai, C. H. Wang, C. C. Ho, *Journal of Alloys and Compounds*. **933** (2023).
107. A. Zhang *et al.*, *Scripta Materialia*. **211** (2022).
108. Y. Ding *et al.*, *Advanced Optical Materials*. **9** (2021).
109. T. Xiao *et al.*, *Materials Chemistry Frontiers*. **5**, 4280–4290 (2021).